Tropical Cyclone Resistance to Strong Environmental Shear

YI DAI,[a] SHARANYA J. MAJUMDAR,[a] AND DAVID S. NOLAN[a]

[a] *Rosenstiel School of Marine and Atmospheric Science, University of Miami, Miami, Florida*

(Manuscript received 5 August 2020, in final form 25 January 2021)

ABSTRACT: It is widely known that strong vertical wind shear (exceeding 10 m s^{-1}) often weakens tropical cyclones (TCs). However, in some circumstances, a TC is able to resist this strong shear and even restrengthen. To better understand this phenomenon, a series of idealized simulations are conducted, followed by a statistical investigation of 40 years of Northern Hemisphere TCs. In the idealized simulations, a TC is embedded within a time-varying point-downscaling framework, which is used to gradually increase the environmental vertical wind shear to 14 m s^{-1} and then hold it constant. This controlled framework also allows for the separation of the TC-induced flow from the prescribed environmental flow. The TC-induced outflow is found to withstand the strong upper-tropospheric environmental flow, and this is manifested in the TC-induced shear difference (TCSD) vector. The TCSD vector, together with the environmental shear vector, defines an azimuthal range within which most of the asymmetric convection is located. The statistical analysis confirms the findings from the idealized simulations, and the results are not strongly sensitive to the TC intensity or basin. Moreover, compared with total shear, the inclusion of TCSD information creates a slightly better correlation with TC intensity change. Overall, the TCSD vector serves as a diagnostic to explain the ability of a TC to resist strong environmental shear through its outflow, and it could potentially be used as a parameter to predict future intensity change.

KEYWORD: Tropical cyclones

1. Introduction

Environmental shear is known to be an important control on tropical cyclone (TC) structure and intensity. Previous studies have focused on the detrimental effects of strong environmental shear on TC intensification (e.g., DeMaria 1996; Frank and Ritchie 2001; Paterson et al. 2005; Tang and Emanuel 2010; Riemer et al. 2010; Nguyen et al. 2017). For example, Simpson and Riehl (1958) first proposed the ventilation of the TC core by dry environmental air at midlevels. Frank and Ritchie (2001) argued that the upper-level warm core was ventilated by the environmental flow, leading to top-down weakening by hydrostatic adjustment of low-level pressure. In addition to the midlevel ventilation, the environment shear can also result in a low-level ventilation by downward flushing of low-entropy air from the middle levels to the boundary layer (e.g., Tang and Emanuel 2010; Riemer et al. 2010).

However, TCs can sometimes intensify under moderately strong shear (5–10 m s^{-1}) and strong shear (>10 m s^{-1}), as revealed in recent studies (e.g., Molinari and Vollaro 2010; Reasor and Eastin 2012; Zawislak et al. 2016; Rios-Berrios and Torn 2017; Ryglicki et al. 2018; Alvey et al. 2020). For example, Molinari and Vollaro (2010) described the rapid downshear reformation of Tropical Storm Gabrielle (2001) under the shear of 13 m s^{-1}. Reasor and Eastin (2012) analyzed the rapidly intensifying Hurricane Guillermo (1997) under the shear of around 8.5 m s^{-1}. Ryglicki et al. (2018) recently documented several TC rapid intensification cases under moderate shear of 5–10 m s^{-1}. In the simulation of Riemer et al. (2010), the TC intensity recovered quickly after the initial weakening under strong shear. Theoretically, a dry TC-like vortex can even resist strong shear for some period of time. Jones (1995) argued that the potential vorticity anomaly interaction between upper and lower levels could lead to cyclonic vortex precession, so that the vortex can be resistant to the environment shear to some extent. Reasor et al. (2004) argued that the tilt asymmetry of the vortex would be damped by radiation of sheared vortex Rossby waves. Recent studies have also identified a reduction in vortex tilt under moderate shear preceding the TC intensification (e.g., Miyamoto and Nolan 2018; Rios-Berrios et al. 2018). Moreover, the diabatic heating and consequent secondary circulation in TCs are thought to greatly enhance that resistance (Zhang and Kieu 2005; Davis et al. 2008).

The question of whether a TC will intensify or weaken under strong shear (>10 m s^{-1}) likely depends on the relative strength of the environmental shear and the TC intensity. This relative strength is difficult to establish, however, since the two factors are physically interconnected. Additionally, in the real atmosphere, it is difficult to isolate the precise role of shear due to competing factors, such as environmental humidity or ocean temperature (e.g., Rios-Berrios and Torn 2017). On the other hand, idealized modeling studies offer the ability to create a controlled environment that strictly isolates the effects of shear. A drawback is that their conclusions may be sensitive to the model configuration. For example, previous idealized simulations have added strong shear onto a weak initial vortex, or shocked the vortex by instantaneously adding the shear.

Corresponding author: Dr. Yi Dai, yidai@lbl.gov

DOI: 10.1175/JAS-D-20-0231.1

© 2021 American Meteorological Society. For information regarding reuse of this content and general copyright information, consult the AMS Copyright Policy (www.ametsoc.org/PUBSReuseLicenses).

Unauthenticated | Downloaded 03/22/25 04:40 PM UTC

Furthermore, the added environmental shear might not maintain its strength or direction during the entire simulation. In this study, we employ a time-varying point-downscaling technique (described in section 2) to smoothly add the environmental shear, and then keep this shear nearly constant through the simulations. In this framework we aim to obtain robust insights into the response (and resistance) of the TC to uniformly strong environmental shear via the adjustment of the TC secondary circulation.

A key motivation of this study arises from our previous studies on the role of TC outflow. The outflow, which is the upper part of the TC secondary circulation, serves as an agent in connecting the upper-level environmental flow with the TC inner-core dynamics (Dai et al. 2017, 2019). Although very important, the outflow is not easy to diagnose. The outflow is often azimuthally asymmetric due to the beta effect and asymmetric environmental flow. Usually, the concentrated region of high wind speed near an altitude of 12 km (or the 200 hPa pressure level) from satellite imagery is used to describe the outflow. This altitude is mostly consistent with findings from aircraft observations (Komaromi and Doyle 2017). However, such a definition is not sufficient to quantitatively relate the full outflow process with TC intensification. We need a simple and meaningful diagnostic to not only represent the direction and strength of the asymmetric outflow, but also to infer the relation between the outflow, environmental flow, and TC intensity.

A central hypothesis of our study is that the TC outflow sometimes becomes adjusted in such a manner that it serves to resist the strong environmental flow. This in turn allows the inner-core TC to develop and intensify. This view of the outflow in opposing and deflecting the environmental flow is built on previous studies (e.g., Elsberry and Jeffries 1996; Dai et al. 2019; Ryglicki et al. 2019). In the observational analysis of Elsberry and Jeffries (1996), a shallow layer of strong upper-level environmental flow could be deflected by the shallow layer of TC outflow. Recently, using an idealized modeling framework, Dai et al. (2019) concluded that the primary TC rainband is a significant source of the outflow, thereby allowing the eyewall to be ''protected'' from the environmental shear flow (in their case, an upper-level westerly jet). In parallel, Ryglicki et al. (2019) used a detailed series of diagnostics to persuasively argue that the unexpected rapid intensification of Hurricane Matthew (2016) was due to its upper-level outflow blocking the moderately strong environmental shear. We note that although the current study shares the similar idea and confirms some features about the outflow in Elsberry and Jeffries (1996) and Ryglicki et al. (2019), we take a different approach by finding a simple representation of the TC upper-level outflow. In this study, we introduce the *TC-induced shear difference* (TCSD) as a quantity to represent the outflow. We view the TCSD as a new diagnostic for understanding the TC resistance to strong environmental shear. By introducing the TCSD, we hope that the outflow can be not only a useful diagnostic to infer the upper-level outflow, but also a nice tool that can be used scientifically and operationally for better understanding and forecasting of TC intensity and structure change.

This paper is organized as follows: Section 2 describes the idealized modeling framework and definitions of shear. The main results of the idealized simulations are presented in section 3, followed by a statistical analysis in section 4 that confirms the findings from the idealized simulations. Conclusions are provided in section 5.

2. Methodology

a. Model configuration

The Weather Research and Forecasting (WRF; Skamarock et al. 2008) Model, version 3.9.1, is used for the idealized simulations. The framework comprises three nested domains with horizontal grid spacings of 18, 6, and 2 km; and domain sizes of 10 800 km × 7200 km, 2298 km × 2298 km, and 768 × 768 km, respectively. In the vertical, 40 equally spaced levels in the WRF normalized hydrostatic pressure coordinate between the surface and approximately 20 km altitude are selected. Doubly periodic boundary conditions are used for lateral boundaries. The WRF single-moment 6-class microphysics scheme (WSM6; Hong and Lim 2006) and the Yonsei University (YSU) planetary boundary layer scheme (Hong et al. 2006) are used. Neither the radiation nor convection scheme are used here. The moist tropical sounding of Dunion (2011) is used in all the simulations. The domainwide sea surface temperature (SST) is set constant at 28°C. The model is on the f plane with a latitude of 25°N. This latitude is chosen to be representative of where a TC can often encounter strong environmental shear. The initial vortex is a modified Rankine vortex with the decay parameter $\alpha = 0.4$, identical to Dai et al. (2017). The initial vortex has a peak tangential wind speed of 20 m s^{-1} at the radius of maximum azimuthal-mean tangential winds (RMW) of 90 km. It also has a Gaussian-like decay in the vertical with the maximum wind speed at $z = 1500$ m. The environmental shear profile and how it is introduced in the model are described below.

b. Time-varying point-downscaling method

The large-scale environmental shear is incorporated into the model using the point-downscaling method (PDS; Nolan 2011). Using PDS, the initial environmental flow is balanced by an artificial force that is added to the momentum equation so that the temperature gradient is no longer needed to balance the thermal wind. Hence, the Coriolis force only acts on the perturbed wind. The initial environmental wind (and therefore the shear) thus changes very little throughout the simulation in the PDS framework, maintaining a persistent and strong environmental flow. This is an advantage over other modeling studies in which the imposed shear weakens with time. Furthermore, since the environmental flow is nearly unchanged, it is easy to separate the TC-induced flow from the total flow (as discussed below in section 2c).

Onderlinde and Nolan (2017) augmented PDS with the new time-varying PDS (TVPDS) framework. The TVPDS is designed to allow time variations of the wind and moisture with time, by a nudging technique introduced by Stauffer and Seaman (1990). Using the TVPDS has the advantage of avoiding the

Unauthenticated | Downloaded 03/22/25 04:40 PM UTC

common problems that arise due to instantaneously adding the shear, such as shocking the TC and failing to realistically spin up an initially weak vortex. The nudging is only performed for the outermost domain ($dx = 18$ km). One limitation in TVPDS, as also mentioned by Finocchio and Majumdar (2017a), is that the nudging can limit TC development by artificially changing TC outflow if the outflow is larger than the intermediate grid ($dx = 6$ km). For that reason, we make the intermediate grid very large (2298 km × 2298 km) to minimize this effect.

For the control (''CTL'') simulation, we use the TVPDS to smoothly add the environmental shear, and turn off the nudging after the shear is imposed for 48 h. This is because after 48 h the shear has already smoothly increased and achieved the expected strength (to be shown below) and the nudging is no longer necessary. An increase of shear to about 14 m s^{-1} in 48 h is consistent with previous studies [e.g., Onderlinde and Nolan (2017) found that a 10 m s^{-1} shear transition needs about 36 h in 44% of the TCs in reanalysis data; Rios-Berrios et al. (2016) also found a decrease of 10 m s^{-1} shear of Hurricane Katia (2011) took about 36 h], although shear transition can occur much faster [e.g., Reasor et al. (2000) found a 10 m s^{-1} shear increase in 3.5 h during Hurricane Olivia (1994)]. Also, turning off the nudging enables the TC outflow (as well as the TC) to develop even more freely. Since TVPDS is a new technique, we have also performed the instantaneous shear simulations (''INS'') under the PDS framework for comparison. Since the main result from the INS simulation is similar to the TVPDS simulation, we will not show many results using instantaneous shear (unless otherwise mentioned).[1]

c. Shear definitions and profiles

A distinctive aspect of this study is that we separate the *environmental shear* from the *total shear*. Their definitions are introduced here. For the idealized simulations, the *total* shear is defined as the 200–850 hPa wind vector difference averaged *within* 500 km of the TC center (defined as the vorticity center at 750 hPa level), and the *environmental* shear is defined as the mean shear *outside* of a 900 km × 900 km box centered on the vortex center. The main results of this study display little sensitivity to different definitions of total and environmental shear using varied distances from the TC center. A central new quantity that we introduce here is the TCSD, defined as the total shear minus the environmental shear. Finally, the *local shear* is defined as the 200–850 hPa wind vector difference averaged within 0–200 km of the center.

[1] In the simulation of instantaneous shear, we still use the older WRF version (V3.4.1, instead of V3.9.1), because in the WRF V3.9.1 test simulation (not shown) of a TC-like vortex developing under a quiescent environment, random convection occurs nearly everywhere at later time. This random convection is able to disrupt the later added shear. The WRF V3.4.1 therefore seems to have a slightly more stable model state compared to V3.9.1, in the modeling of the instantaneous shear in the PDS framework. We also note that the TVPDS test in WRF V3.4.1 also has very similar results compared to those in V3.9.1 (not shown).

In section 3e, we will also investigate two real cases: Hurricanes Edouard (2014) and Matthew (2016), both of which intensified in moderately high shear. To show the outflow of these two real cases, we use the upper-level atmospheric motion vectors (AMVs; Velden et al. 1997), together with geostationary (GOES) water vapor satellite imagery, collected from the Cooperative Institute for Meteorological Satellite Studies (CIMSS) at the University of Wisconsin–Madison. In section 4, we will also provide a statistical analysis of real TCs. For consistency with operational use in these real cases, the total shear is defined in these sections as the 200–850 hPa wind vector difference averaged within 500 km of the center, and the environmental shear is simply defined as the 200–850 hPa wind vector difference averaged within 500–1000 km of the center. The data used to calculate the shear vectors for real TCs are from the European Centre for Medium-Range Weather Forecasts (ECMWF) interim reanalysis (ERA-Interim; Dee et al. 2011), with a horizontal resolution of about 0.7° × 0.7°.

The vertical profile of the environmental westerly shear prescribed in the control simulation is adapted from the westerly jet profile in Dai et al. (2017). We only keep the vertical variation of the jet (no meridional variation) and set the maximum wind as 15 m s^{-1} at approximately 200 hPa. We have also performed sensitivity simulations using two different types of westerly shear profiles from Finocchio and Majumdar (2017b). These two types of shear profiles are representative of the composite deeply distributed shear (DDS) and shallow upper-level shear (SUS) profiles derived from reanalysis data (Finocchio and Majumdar 2017b). We note that our result is not sensitive to these different shear profiles (as will be shown below).

3. Results

a. General evolution

The TC in the CTL simulation is first allowed to intensify into a strong hurricane in the absence of shear (black solid line between −96 and 0 h in Fig. 1). The TVPDS method is then used to gradually introduce the environmental shear (~14 m s^{-1}) from 0 h, which is the reference time for all the analyses in this paper. Since the initial shear is very weak, the vortex still intensifies during the first 12 h. The vortex then starts to fill, and quickly weakens when the environmental (and total) shear exceeds 10 m s^{-1} after 24 h (to be shown later). Around 42–48 h, the TC reaches a local maximum of minimum sea level pressure (MSLP), and then it gradually reintensifies through to the end of the simulation (144 h). We call this reintensification (following the TC weakening under shear) TC recovery. Since the TVPDS nudging is also turned off at 48 h, it is worth confirming whether or not the reintensification is due to the terminated nudging. To investigate this, another simulation ''NudgeOn'' (black dashed line in Fig. 1), which is identical to CTL except that the nudging is kept on until the end of the simulation, also starts to reintensify the TC at approximately $t = 48$ h, albeit at a slower rate than CTL. We therefore conclude that the reintensification in the CTL is not an artifact of the termination of the nudging.

Unauthenticated | Downloaded 03/22/25 04:40 PM UTC

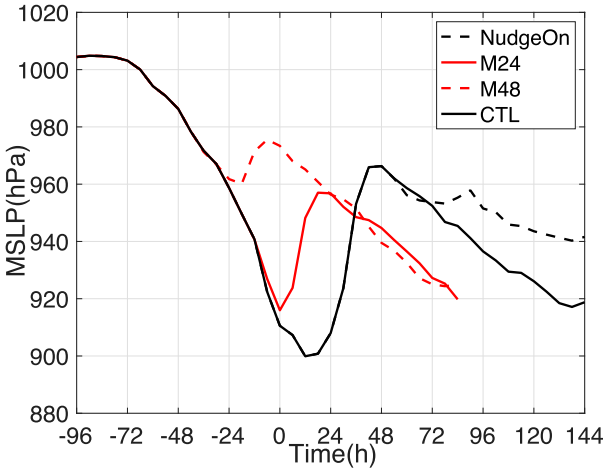

FIG. 1. Time series of minimum sea level pressure (MSLP) for CTL (black solid line), NudgeOn (black dashed line, where we kept the nudging to the end of the simulation at $t = 144$ h), M24 (red solid line, where it is as in CTL, except shear is added 24 h earlier than CTL), and M48 (red dashed line, where it is as in CTL, except shear is added 48 h earlier than CTL). Note that both M24 and M48 are only run to $t = 84$ h to save computation and storage.

b. *Robustness of the recovery*

The recovery might also be due to the vortex already being very strong when the shear starts to increase. To test that sensitivity, we perform two additional simulations in which the shear is added at earlier times. M24 (red solid line in Fig. 1) is where the shear is added 24 h earlier than CTL, while M48 (red dashed line in Fig. 1) is where shear is added 48 h earlier than CTL.[2] These two simulations indicate that weaker (before the weakening) TC vortices can also reintensify under strong shear. We have also performed similar simulations for instantaneous shear (not shown), but they did not experience the recovery. These results suggest that a vortex needs a relatively strong intensity to resist the shocking effect of instantaneous shear.

We note that while Onderlinde and Nolan (2017) used a similar shear strength to ours in their initial TPVDS simulation, their TC did not reintensify. The results here are different because we have greatly increased the size of the intermediate grid ($dx = 6$ km, 2298 km here vs 720 km in their study). As mentioned in section 2b, the nudging used in TVPDS strongly regulates the large-scale flow in the outermost domain ($dx = 18$ km). When the middle domain is small, the development of the outflow is heavily limited once the outflow expands outside the middle domain, thereby restricting the TC secondary circulation and thus TC intensity. In other words, the difference between our study here and Onderlinde and Nolan (2017) suggests that the upper-level outflow is an important factor for TC intensity change, and thus needs to be simulated appropriately.

[2] Note that in order to save computation and storage, both M24 and M48 have only been simulated to $t = 84$ h.

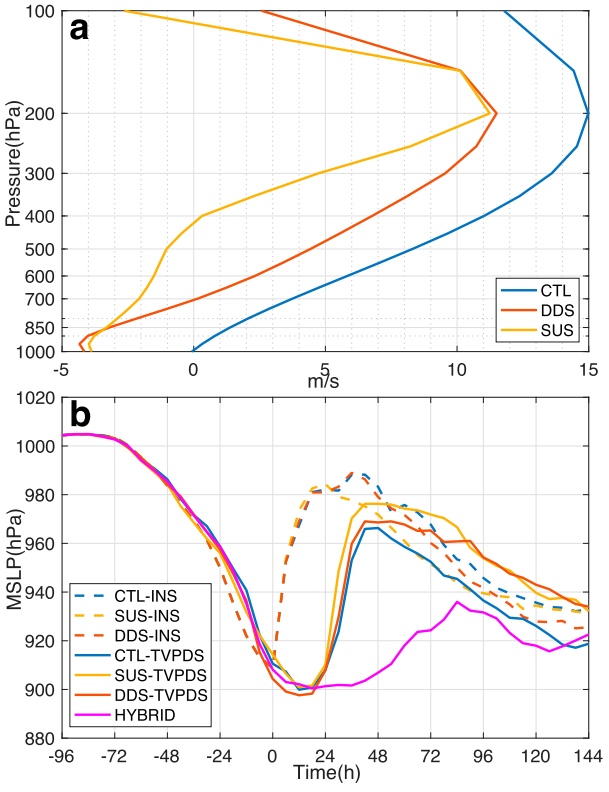

FIG. 2. (a) Vertical profiles of the environmental shear. Blue line is the shear used in CTL. The red and orange lines respectively indicate the composite deep-layer shear (DDS) and shallow-layer shear (SUS) used in Finocchio and Majumdar (2017b). (b) Time series of MSLP for instantaneous (INS; dashed line) and TVPDS (solid line) simulations using different shear profiles. HYBRID (magenta) represents an experiment where we smoothly added the shear, but also included the meridional temperature gradient to balance the vertical shear.

The reintensification in CTL might also be sensitive to the profile of shear. However, our simulations using different realistic shear profiles (CTL, SUS, and DDS, Fig. 2a) in both the TVPDS and INS frameworks show that they all experienced reintensification (Fig. 2b). The reintensification under strong environmental shear is thus robust to realistic changes in the shear profiles. It is noteworthy that the result here seems not to be sensitive to shear depth, which has been proposed (e.g., Finocchio et al. 2016; Ryglicki et al. 2019) to modulate the effects of shear. This different result here could either imply that the consistency between the outflow-layer height and the top of the shear profile is more important than shear depth, or is simply due to differences in the model configurations. The final sensitivity experiment to test the robustness is called HYBRID. Unlike the PDS and TVPDS simulations, the HYBRID simulations balance the zonal wind field with a temperature gradient computed from thermal wind. The wind shear is changed over time with a similar nudging process, that also acts in concert on the necessary baroclinic temperature gradient. As Nolan (2011) found when comparing this "balanced shear" to the PDS method, the vortex is more

Unauthenticated | Downloaded 03/22/25 04:40 PM UTC

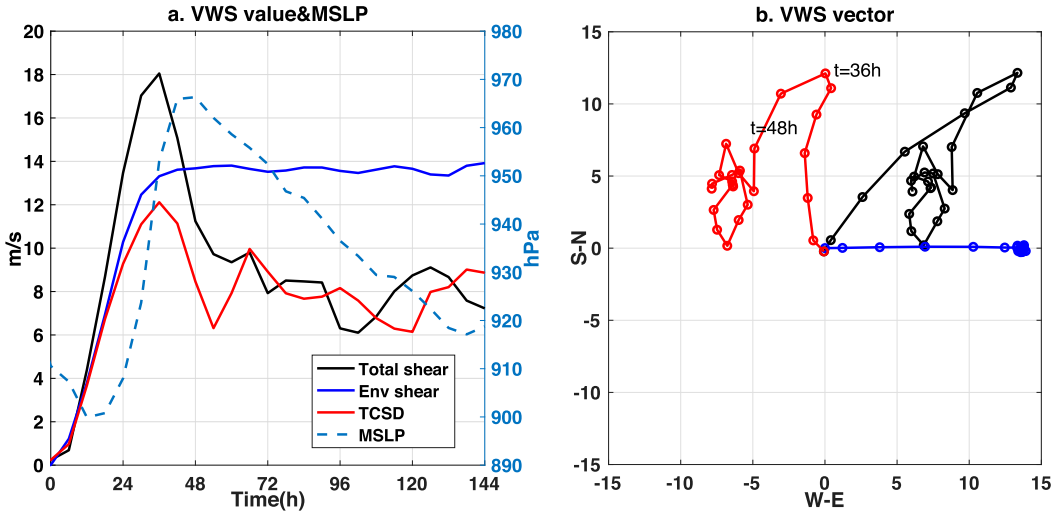

FIG. 3. Time evolutions of (a) shear value and (b) shear vector for the total shear (solid black curve), environmental shear (blue curve), and TCSD (red curve, defined as total shear minus the environmental shear). The time evolution of MSLP (dashed light blue curve) is also shown in (a). The time interval is 6 h.

resistant to the shear with the balanced temperature gradient (magenta line in Fig. 2b). The HYBRID simulation also agrees with previous studies that only used balanced and instantaneous shear, in which the TC started to recover at pretty strong intensity [such as Vmax $\sim$ 65 m s^{-1} in Riemer et al. (2010), their 15 m s^{-1} shear case], which is possibly a result of the environmental shear being weakened due to horizontal reduction of the temperature gradient by the TC circulation. We found that the environmental shear in HYBRID remains close to 10 m s^{-1} during the simulation. This again demonstrates the advantage of using PDS to keep the environmental shear nearly constant with time.

c. *TCSD*

The asymmetric upper-tropospheric outflow is a response of the TC to the environmental shear. Subtracting the environmental shear from the total shear creates a vector, the TCSD, that corresponds to the TC-relative asymmetric shear, which we hypothesize is dominated by the outflow in most cases. Therefore, introducing TCSD is a simple way to explore the relationship between environmental flow, outflow, and TC intensity change.

Here, we show the time evolutions of total shear, environmental shear, and TCSD in CTL. We note that the TCSD and local shear are different (to be shown below), because local shear captures information about the innermost asymmetric wind near the eyewall, while the TCSD is more representative of the larger-scale TC wind information, such as the outflow. By design in TVPDS, the environmental shear increases smoothly from 0 to about 14 m s^{-1} during the first 48 h, and then stays at that value until the end of the 144-h simulation (blue line in Fig. 3a). There is a small oscillation (less than 1 m s^{-1}) of the environmental shear, which is likely a result of the TC outflow channel expanding outside the defined 900 km $\times$ 900 km box. The TC total shear (black solid line in Fig. 3a) as well as the TCSD (red line in Fig. 3a) increase rapidly along with the environmental shear during the first 40 h of adding shear. At t = 36 h, the total shear reaches a maximum of about 18 m s^{-1} and then quickly decreases. The value of TCSD experiences substantial oscillations after reaching the maximum value of about 12 m s^{-1} at 36 h, with an average value of about 8 m s^{-1} after this time. The reintensification (MSLP, light blue dashed line in Fig. 3a) starts after the total shear is already decreasing.

The shear magnitude does not tell the entire story. After some adjustment, the direction of the total shear remains toward the northeast (NE), while the TCSD remains toward the northwest (NW) direction (Fig. 3b), making the angle between TCSD and environmental shear larger than 90° during the recovery stage. The zonal component of the TCSD is usually negative and thus upshear. This suggests that the TC-induced wind shear, potentially a consequence of the upper-tropospheric outflow, is able to partially counteract the westerly environmental wind shear. From Fig. 3, it is not until the TCSD vector begins to increase its upshear component (36 h, Fig. 3b) that the total shear value starts to decrease (Fig. 3a). Such a configuration of the TCSD vector seems important to the recovery of the TC. A natural question to ask is: how does the TCSD physically describe the outflow?

To answer that question, we first investigate the inertial stability. Relative to the center of a vortex, the inertial stability is defined as: $I^2 = (f + V/r)(f + \zeta)$, where f is the Coriolis parameter, V the tangential wind, r the distance to the TC center, and ζ the vertical component of relative vorticity. Adding a westerly uniform wind in the upper troposphere is equal to decreasing V to the north and increasing V to the south of the TC center. As a result, I is weakened in the north and enhanced in the south. The azimuthally asymmetric distribution of I can result in an asymmetric upper-tropospheric TC wind distribution (see also Fig. 10 in Dai et al. 2019). Figure 4a shows the 200 hPa inertial stability I at t = 48 h. It is clear in Fig. 4a that I is low in the NW quadrant beyond around 200 km of the TC center, consistent with our expectation above. Within 200 km of the

Unauthenticated | Downloaded 03/22/25 04:40 PM UTC

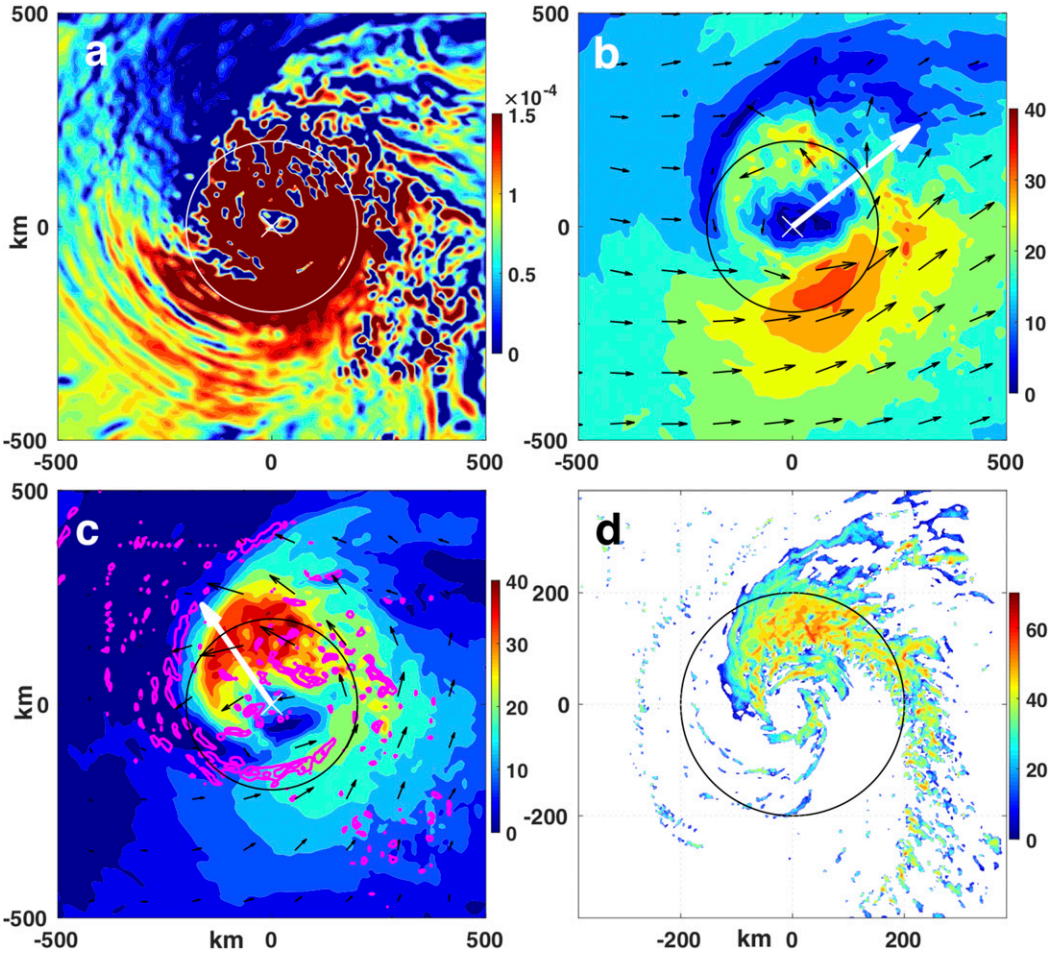

FIG. 4. The horizontal field of (a) inertial stability (I, s^{-1}; note that wherever $I^2 < 0$, we set $I = 0$), (b) total horizontal wind speed (along with wind vectors), and (c) TC-only wind speed (along with wind vectors) at 200 hPa at $t = 48$ h in CTL. The TC-only wind is defined as the total wind minus the environmental wind, and the environmental wind is the mean wind outside of a 900 km × 900 km box centered on the vortex center. Magenta contours in (c) represent convergence (-4×10^{-4} and -2×10^{-4} s^{-1}, respectively). White vectors in (b) and (c) represent total shear vector and TCSD, respectively. (d) The inner-core reflectivity at $p = 850$ hPa at $t = 48$ h. The $r = 200$ km circle is also shown in each subplot.

center, scattered low I also occurs in the NW quadrant, a result of convection in the rainband (Fig. 4d). This configuration of I promotes the escape of TC air radially outwards to the NW quadrant. Also shown are the total wind (Fig. 4b) and TC-only wind field (Fig. 4c) which is defined as the total flow minus the environmental flow. The environmental flow is also defined as the mean flow outside of a 900 km × 900 km box centered on the vortex center, similar to the style of the definition of environmental shear. The total wind has its westerly maximum to the south of the TC center (Fig. 4b). However, the TC-only wind (Fig. 4c) has strong easterly outflow to the north and especially the NW quadrant, effectively resisting the upper-tropospheric environmental wind that is coming from the west. It is noteworthy that our result here is very similar to Komaromi and Doyle (2018), where a TC interacts with a trough that is inducing southwesterly shear in the beta plane. In their Fig. 9, I is also to the NW of the TC. In addition, their calculated ageostrophic wind is consistent with our TC-only wind that corresponds to the region of lowest I. The preferential location of the enhanced TC-only wind in Fig. 4c corresponds closely to the asymmetric convective rainband below (Fig. 4d), consistent with the main result of Dai et al. (2019) that the rainband is an important source of TC upper-troposphere outflow, and they evolve together in response to the environmental flow. Along the periphery of the strong TC-only wind gradient is where the TC outflow and environmental flow converge, as indicated by the magenta convergence contours to the west of the TC center (Fig. 4c). This convergence region might be similar to the region of confluence upshear of the TC by the interaction between TC outflow and environmental flow observed by Ryglicki et al. (2019). That convergence will dynamically force a mesoscale downdraft (to be shown later).

We therefore suggest that the enhanced TC outflow in the NW quadrant is a response of the upper-tropospheric flow in

Unauthenticated | Downloaded 03/22/25 04:40 PM UTC

the TC to the westerly environmental wind, and that the NW location preferentially helps the TC resist the detrimental effect of the strong environmental flow. By definition, the TCSD (white vector in Fig. 4c) is the area average of that TC-only flow, thus nicely representing the general location and direction of the TC-induced asymmetric outflow.

d. Weakening and recovery

Here we will focus on the period of 0 to 72 h, from the imposition of the shear to when the TC is recovering steadily. Figure 5 shows a Hovmöller diagram of the azimuthal-mean tangential wind at $z = 1$ km, where the strongest tangential wind is approximately located. The vortex does not weaken during the first 12 h because the environmental shear is still weak. Between approximately 12–36 h, the azimuthal-mean wind field at and outside the RMW (~30–40 km) decays slowly. Over the next 12 h, the eyewall collapses and the RMW accordingly expands with large oscillations. After around $t = 48$ h, the TC starts recovering with a slightly larger RMW (~50–60 km) than before the weakening. The maximum azimuthal-mean tangential wind also begins to increase gradually, although not as quickly as during the initial intensification (not shown). Note that the recovery also comes with an expansion of the tangential wind field outside the RMW, potentially increasing the destructiveness of the TC wind.

It is well understood that vertical wind shear can induce a strong asymmetry in the dynamic and thermodynamic structure around the TC inner-core region (e.g., Jones 1995; Corbosiero and Molinari 2002; Riemer et al. 2010). We now focus on the asymmetry induced by the environmental flow, and explore its impacts on the TC structure change. First, we introduce the "forced downdraft," which is a mesoscale feature just below the location of upper-tropospheric wind convergence created by the environmental flow and the TC-induced flow (Fig. 4c) that moves radially inward (black vectors in Fig. 6 indicates radial wind), and descends from approximately $z = 10$ km all the way down to the boundary layer (Fig. 6). This forced downdraft is adjacent to the convective updraft, and forms a physical boundary of the convection. We call it a forced downdraft because this downdraft originates from the converging flow between the TC outflow and westerly environmental flow in the upper-level, and is then sustained by diabatic cooling due to evaporation. Consistent with Dai et al. (2019), we view the forced downdraft, the upper-level outflow, and the convective rainband as a whole system, which together is a response of the TC to strong environmental flow. At $t = 37$ h (upper panels of Figs. 6 and 7), the forced downdraft is relatively close to the TC center. Concurrently, the TC-relative radial inflow is very strong and there is no outflow upshear at $z = 10$ km (Fig. 6a). At $t = 43$ h (lower panels of Fig. 6), convection (red shading in Fig. 6 indicates diabatic heating) is better developed upshear, and the forced downdraft that is adjacent (radially outside) of the convective region is not as close to the TC center. At the same time, some part of the upper-level outflow is evident at 10 km height also (Fig. 6d). It is noteworthy that our forced downdraft may be different from the "descending inflow" as observed by Didlake et al. (2018) in the rainband of Hurricane Earl (2010), because their

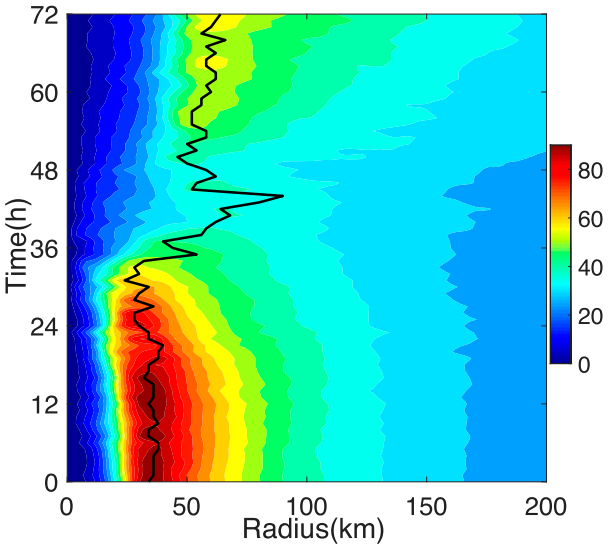

FIG. 5. Hovmöller diagrams of azimuthal-mean tangential wind ($m\,s^{-1}$) at $z = 1$ km within 300 km to the TC center from $t = 0$ to 72 h in CTL. The radius of maximum azimuthal-mean tangential wind is shown as a black curve.

"descending inflow" originates from the diabatic cooling within the midtroposphere stratiform region and the downdraft strength is about $-1\,m\,s^{-1}$ (their Fig. 7), while our forced downdraft originates at around 10 km height with downward velocities reaching $-10\,m\,s^{-1}$. This difference may be a result of stronger environmental shear in our case. Downdrafts with such large magnitude in TCs have been observed before, such as by Black et al. (1996), Guimond et al. (2010), and Rogers et al. (2012). Moreover, our result is supported by the simulations of Riemer et al. (2010), where the downdraft brought the downward flushing of low entropy air to the boundary layer. From their Fig. 18, downdrafts appear to also originate from the upper levels at approximately $z = 10$ km, even though the minimum θ_e was located in the midtroposphere. In the recent observational study of Ryglicki et al. (2018), they found a location of thin arcs in the water vapor imagery as a common feature upshear of TCs which have experienced intensification under moderately strong shear. We hypothesize that the thin arcs indicate the location where the forced downdraft originates in the upper troposphere, because water vapor could vary a lot near the origin of the forced downdraft. Therefore, using the forced downdraft as a pathway, we are able to connect the TC lower boundary layer with the strong upper-level environmental flow, and we are able to see how the TC inner core is affected by the environmental flow through this forced downdraft just below the outflow layer.

Because the forced downdraft brings dry air from above, it serves as a thermodynamic constraint on the vortex (as suggested by Riemer et al. 2010). At the stage of rapid weakening at 37 h (Fig. 7a), the dry air intrusion from the upper troposphere and radially inward (red vectors in Fig. 7) to TC center is very strong. The forced downdraft is so close to the TC center ($x = 0$) that dry air in the eye and dry air associated with the shear are nearly connected to each other (white shading in

Unauthenticated | Downloaded 03/22/25 04:40 PM UTC

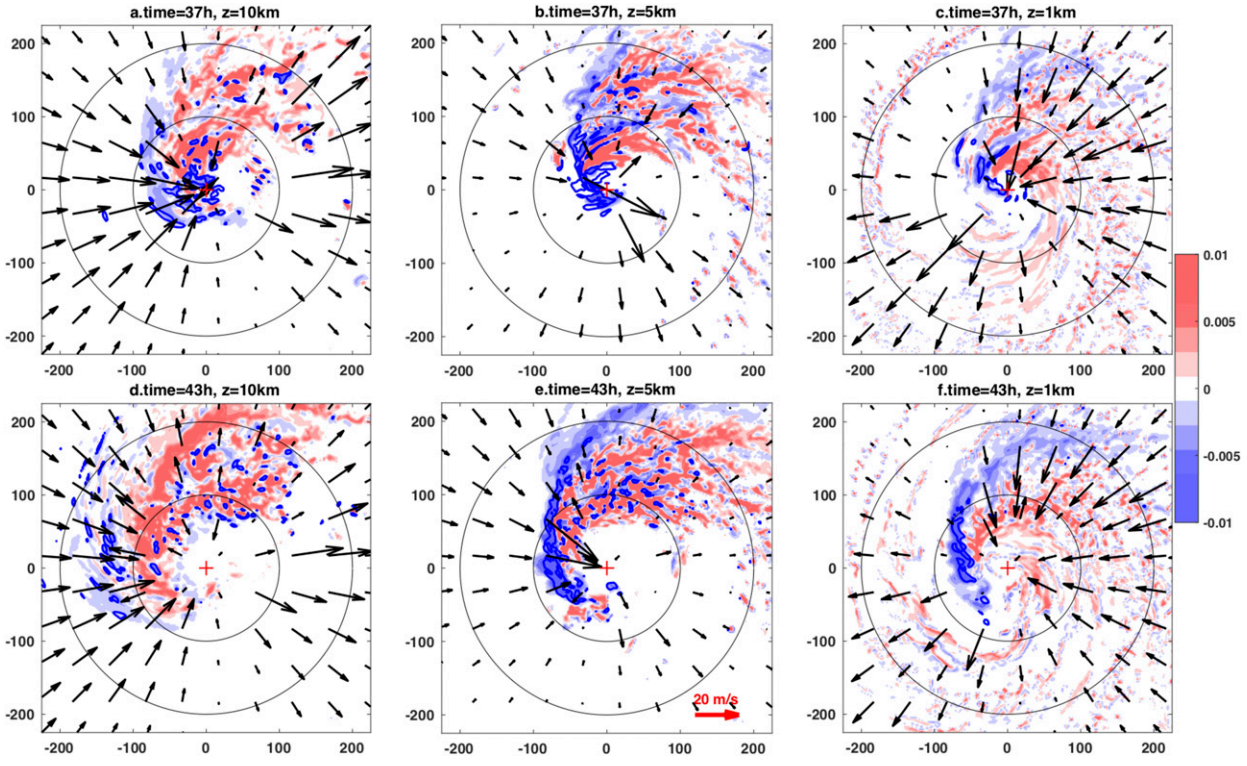

FIG. 6. The radial wind (vectors), downdrafts (dark blue contours show -8 and $-2\,\mathrm{m\,s^{-1}}$), and diabatic heating rate ($\mathrm{K\,s^{-1}}$, shading) at $t = 37$ h in the control simulation for z = (a) 10, (b) 5, and (c) 1 km. (d)–(f) As in (a)–(c), but at $t = 43$ h. The $r = 100$ and 200 km circles are also shown in each subplot.

Fig. 7a). The close distance between the dry downdraft and the eyewall also limits the recovery of the dry air from surface fluxes before it enters the updraft. The TC outflow is weak and concentrated above $z = 12$ km. The mesoscale forced downdraft in Fig. 7b (around $x = -50$ km) is more slantwise than the convective downdraft/updraft (around $x = 30$–70 km) in the rainband. Note also the large magnitude of the downdraft: the strongest downdraft is stronger than $-10\,\mathrm{m\,s^{-1}}$, two orders of magnitude larger than the dynamically induced dry downdrafts discussed in Jones (1995) and Zhang and Kieu (2005). At $t = 39$ h, the forced downdraft is still close to the eye (Fig. 7b), so that the vortex is still weakening. It is not until the forced downdraft is gradually pushed outside the inner-core region (beyond 50 km of the center) by the expansion of the upper-level TC enhanced outflow at $t = 41$ h (Fig. 7c) that the dry air (low entropy) is able to recover before moving to the eyewall. Around $t = 41$ h, the vortex reaches its weakest intensity indicated by MSLP (Fig. 3a), and after that the vortex starts to recover. The inner-core region (within 50 km) starts to gain moisture at 43 h as the upper-tropospheric outflow gets stronger and more organized (Fig. 7d), and after that time more convection is initiated and the eyewall is able to close itself by axisymmetrizing the convection (not shown). From the evolution of TCSD direction (red curve in Fig. 3b; we only have the 6-h wind data for outer domain because of storage limits) at this stage (from 37 to 43 h), TCSD turns cyclonically quickly from northward to nearly northwestward, indicating the expansion of outflow upshear (Fig. 6a vs Fig. 6d) and increasing resistance to environmental shear. The $z = 1$–6 km vortex tilt (defined as the displacement of the smoothed vorticity centroid in between) is also calculated at $t = 37$ and 43 h, but we did not find much difference as the tilt is almost always about 30 km to the north, consistent with the azimuthal position of the convective region (Fig. 6b vs Fig. 6e).

e. TCSD as an indicator of TC intensification

When convective cells move from the downshear-left to upshear-left quadrants under the influence of shear, a TC will often start intensifying (e.g., Zhang and Tao 2013; Rogers et al. 2016; Rios-Berrios et al. 2018). Perhaps the main reason is that the upshear-left convection is radially closer to the eye than downshear left, so that the diabatic heating effect is more efficient to spin up the vortex (Nolan et al. 2007; Rogers et al. 2016). In our case here, the TCSD is to the upshear left of the environmental shear vector when the TC is recovering (Fig. 3b). Therefore, our view of TCSD indicating TC intensification is consistent with those studies using the location of convection to indicate TC intensification. Based on the analysis in section 3c, the TCSD being upshear left of the environmental shear is physically significant, because in that configuration, the TC-induced flow can effectively resist strong environmental flow. Also, the larger the angle between the TCSD and environmental flow, the more the TC-induced flow is opposite to the environmental flow (the magnitude of

Unauthenticated | Downloaded 03/22/25 04:40 PM UTC

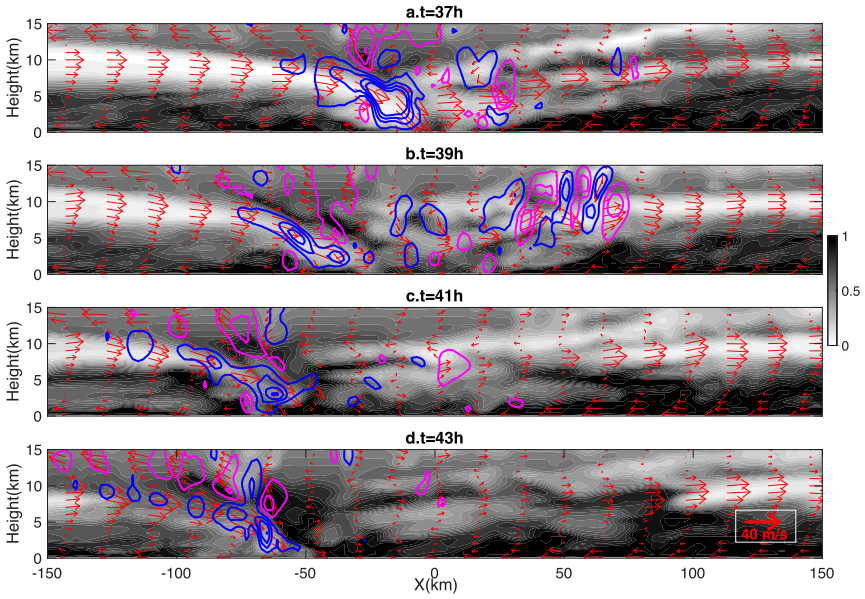

FIG. 7. West–east vertical cross section of the vortex center at t = (a) 37, (b) 39, (c) 41, and (d) 43 h in CTL. The shading represents relative humidity (white means dry air). Red vectors indicate the vertical secondary circulation (radial and vertical wind). Downdrafts of −11, −8, −5, and −2 m s^{-1} are indicated by blue contours, while updrafts of 2, 5, 8, and 11 m s^{-1} are indicated by magenta contours.

TCSD being the same). We next use two real hurricanes to provide examples of our argument.

Hurricanes Edouard (2014; Stewart 2014) and Matthew (2016; Stewart 2017) were both major hurricanes that experienced rapid intensification[3] (RI) in the Atlantic basin, although Matthew intensified at a much faster rate than Edouard. During the periods of RI, their surrounding environmental shear was strong and not typically favorable for intensification. Table 1 shows that the environmental shear around Edouard was about 10 m s^{-1} during its RI, and Matthew experienced environmental shear of about 13 m s^{-1} during its RI. Such "unexpected" intensification might be understood using TCSD. During its short period of RI (0600–1200 UTC 14 September 2014), Edouard had a total shear of about 7.5 m s^{-1} instead of 10 m s^{-1} (environmental shear). To visualize the TCSD, we show upper-level AMVs (Velden et al. 1997) of Edouard and Matthew during their intensification periods in Fig. 8. First, by comparing the upper panels with lower panels, the TCSD in Fig. 8a nicely represents the southeasterly outflow (blue wind barbs in Fig. 8c) for Edouard to the northwest of the center, and TCSD Fig. 8b illustrates the northeasterly outflow (blue wind barbs in Fig. 8d) for Matthew to the southwest of the center. Therefore, the TCSD is strongly correlated with the upper-level outflow. The upper-level outflow outside the eyewall of Edouard was highly asymmetric on 1200 UTC 14 September 2014 (Fig. 8c). The asymmetric outflow created a west-northwestward TCSD, located upshear left of the environmental shear vector with an angle of about 130° and a magnitude of about 7 m s^{-1}, keeping the total shear below 8.5 m s^{-1}. Matthew is a more extreme case: its environmental shear was nearly 14 m s^{-1} on 1200 UTC 30 September 2016, while its intensification rate was 3 times that of Edouard (Table 1). The TCSD might help explain this puzzle: in this case, the TCSD is almost opposite to the environmental shear (Fig. 8b), greatly alleviating the detrimental shear effect on Matthew (total shear is only 8 m s^{-1}). With the help of other favorable conditions, such as a high sea surface temperature, Matthew rapidly intensified (note that the latitude of Matthew at the time of interest was much lower than that of Edouard). These two hurricane cases motivate a more thorough statistical study of the relationship between TCSD and TC intensification.

f. TCSD as a lateral boundary of asymmetric convection

Another interesting finding of TCSD is that it can represent where the asymmetric convection is located. Previous studies indicate that the downshear left of the total shear is usually the place where asymmetric convection is located under shear (e.g., Black et al. 2002; Corbosiero and Molinari 2002; Rogers et al. 2003). Another indicator of the convection location is by the "downtilt direction" (e.g., Davis et al. 2008; Reasor et al. 2013), which defines the direction where the vortex tilts the most under shear. Such approximations of the convection location are useful, but just using one vector to define the location is somewhat tricky: convection does not always cover exactly one

[3] Based on the AMS Glossary, rapid intensification is defined as the increase in the maximum sustained wind of at least 30 kt in a 24-h period. Following this intensification rate (7.5 kt in 6 h), we claim that Hurricane Edouard (2014) also experienced a very short period of rapid intensification during 0600–1200 UTC 14 September 2014.

Unauthenticated | Downloaded 03/22/25 04:40 PM UTC

TABLE 1. Evolutions of Hurricanes Edouard (2014) and Matthew (2016) during their early quick intensification stage. Shown here are time, total shear, environmental shear, TCSD, and Vmax.

Name	Time and date	Total shear ($m\,s^{-1}$)	Environmental shear ($m\ s^{-1}$)	TCSD ($m\,s^{-1}$)	Vmax (kt)
Edouard	0000 UTC 14 Sep 2014	8.8	12.4	5.2	55
Edouard	0600 UTC 14 Sep 2014	7.3	10.4	7.1	60
Edouard	1200 UTC 14 Sep 2014	8.1	9.9	6.8	70
Edouard	1800 UTC 14 Sep 2014	8.0	10.6	10.2	75
Matthew	0000 UTC 30 Sep 2016	8.1	11.0	3.1	70
Matthew	0600 UTC 30 Sep 2016	9.7	11.8	2.4	85
Matthew	1200 UTC 30 Sep 2016	8.2	13.3	5.2	100
Matthew	1800 UTC 30 Sep 2016	7.6	13.3	5.7	120

quadrant. Can we find another vector to define the location and azimuthal range of the convection?

As already discussed in section 3c, the TCSD serves as an indicator of the upper-tropospheric asymmetric outflow. The interaction between the outflow and environmental flow results in converged air being forced downward (Fig. 4c), which is the origin of the forced downdraft. This downdraft is adjacent to the TC inner-core convective updraft (Fig. 6), thus

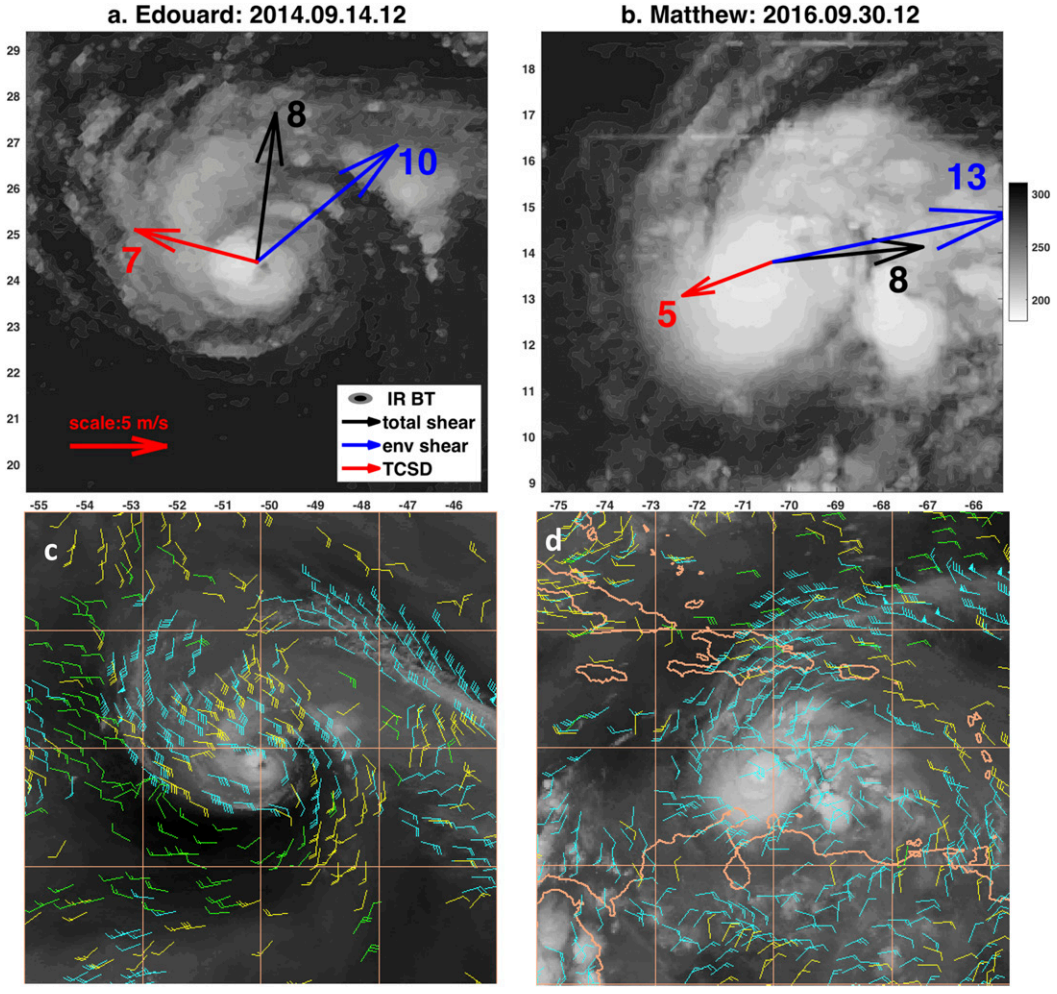

FIG. 8. Snapshots of GOES infrared brightness temperature (shading) for (a) Hurricane Edouard (2014) and (b) Hurricane Matthew (2016). Red vector indicates TCSD, black vector indicates total shear, and blue vector indicates environmental shear. The numbers near the vectors are their shear values. Also shown are the upper-level atmospheric motion vectors (AMVs; blue wind barbs indicate wind at 100–250 hPa) superposed one the GOES-East water vapor images for (c) Edouard and (d) Matthew. Note that the domain size of (c) and (d) for each boundary are 20°, about twice the size of those in (a) and (b).

Unauthenticated | Downloaded 03/22/25 04:40 PM UTC

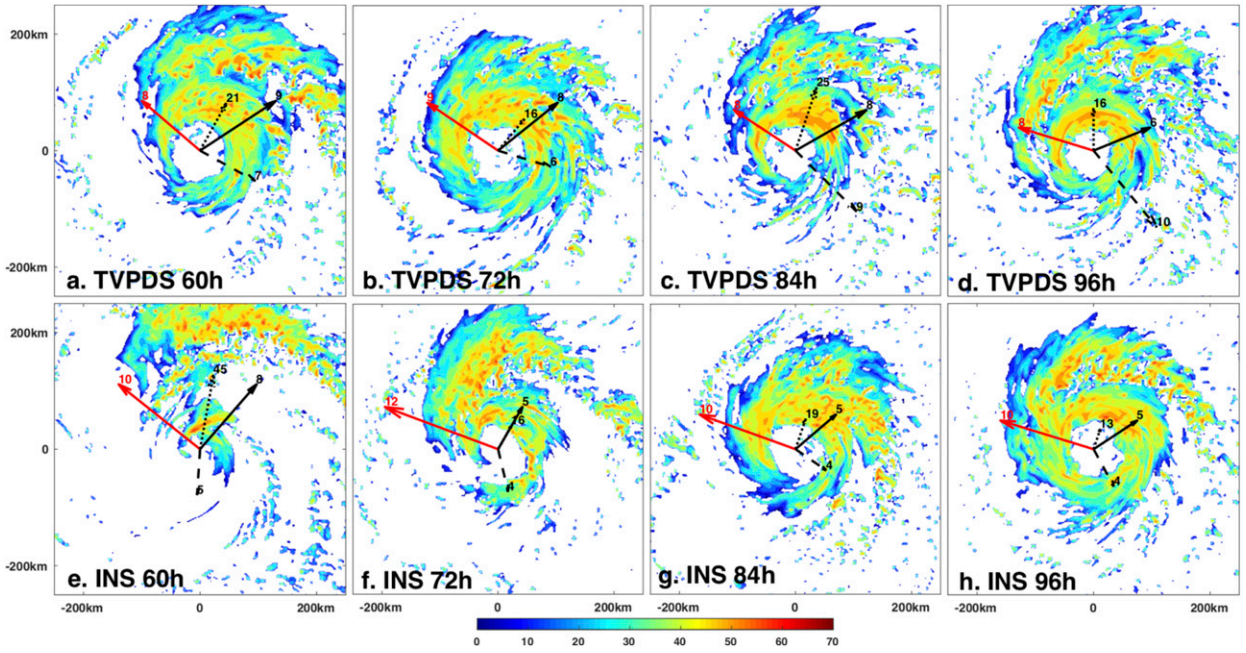

FIG. 9. (a)–(d) Snapshots of reflectivity at $p = 850$ hPa for CTL at $t = 60, 72, 84$, and 96 h. Solid black vector indicates total shear (m s^{-1}), and the solid red vector indicates TC-induced shear difference (TCSD; m s^{-1}). Dotted black vector indicates the tilt (km, between 400 and 900 hPa), and the dashed black vector indicates the local shear (m s^{-1}). Numbers hear the vectors are either shear value or tilt magnitude. For better visualization, the length scaling of tilt is different from shear value. (e)–(h) As in (a)–(d), but for the simulation with the instantaneous shear. Note that environmental shear is always westerly.

serving as a physical lateral boundary of the asymmetric convection. The TCSD represents a general location where the asymmetric convective cells end, or merge with the eyewall. In other words, the upper-tropospheric outflow (indicated by TCSD), the forced downdraft, and the asymmetric inner-core convection coexist as a response to the upper-level environmental flow. Therefore, using the TCSD to represent the location of the asymmetric convection is physically reasonable. By combining both the TCSD and environmental shear, the asymmetric convection around the TC can be physically represented, with most of the convection located between the TCSD and environmental shear vector (Fig. 9). Figure 9 demonstrates this idea using both the CTL and INS simulations. To compare with previous ideas about the region of convection, we have also presented the tilt vector (the displacement of the smoothed vorticity centroid between 400 and 900 hPa; dotted black vector in Fig. 9), and local shear vector (dashed black vector in Fig. 9). From the snapshots of reflectivity in Fig. 9, it is clear that the TCSD (solid red vector in Fig. 9) approximately defines a lateral boundary of the asymmetric convective area, and most of the convection (roughly defined as where reflectivity > 45 dBZ in Fig. 9) is always located between the TCSD vector and the environmental shear vector (always pointing east in these figures). The downshear left of total shear (solid black vector in Fig. 9) is generally good to describe the location of the asymmetric convection, but in a few cases that region is not representative enough, such as in Figs. 9d and 9g. The tilt vector is always between the environmental shear and TCSD, indicating that our idea of the asymmetric convection location is consistent with the "downtilt" theory (Davis et al. 2008; Reasor et al. 2013). But occasionally, the "downtilt" region does not represent the majority of convection, as shown in Fig. 9f. Consistent with the observation in Reasor et al. (2013), the local shear is always to the right of the total shear [we have also calculated local shear in a tilt-relative framework as in Reasor et al. (2013), and found this result does not change, although the angle between total shear and local shear becomes smaller than Fig. 9]. Therefore, the local shear is more of a vector reflecting the TC asymmetry in the very inner core, and might not reflect the general mesoscale asymmetric convection around the TC.

Based on both Fig. 9 and the examples of Hurricanes Edouard (2014) and Matthew (2016) in Fig. 8, TCSD seems good at defining the downwind boundary of the region of asymmetric convection. We next provide more cases to test this hypothesis. If proven to be true, TCSD could serve as a useful tool to diagnose the asymmetric convection around TCs, perhaps more so than the downshear-left quadrant. Such regions of asymmetric convection are always accompanied by strong winds and precipitation.

4. Statistical analysis of TCSD

a. TCSD, convection coverage, and shear resistance

To investigate whether the above arguments can be generalized, we perform a statistical analysis. The vertical wind shear vectors are computed using the ERA-Interim data, with a

Unauthenticated | Downloaded 03/22/25 04:40 PM UTC

horizontal grid spacing of about 0.7° × 0.7°. The time range of the data is from 1980 to 2019 (note that the last day for 2019 is 31 August due to data availability). The TC center and intensity data are from the International Best Track Archive for Climate Stewardship (IBTrACS; version 4). To gain information about convection, we use the gridded infrared brightness temperature (Knapp et al. 2014), which has a horizontal resolution of 0.07° × 0.07°. We define convective clouds where the brightness temperature is less than 250 K, within a region that is less than 3° radially (approximately 300 km) relative to the TC center. Based on Fig. 8 in this paper and Fig. 3 of Fischer et al. (2017), 250 K is an appropriate value to define active convection. Discussions using a smaller value to define convection will be shown below. All the data are six hourly. Some criteria are used to select the data. For example, we only use data from TCs that are equatorward of 40°N, do not make landfall within 6 h, and have a maximum sustained wind speed equal to or above tropical storm strength [34 kt (1 kt $\approx$ 0.51 m s^{-1})]. An important metric in this section is the angle between different vectors. Here, we use the environmental shear as the base vector that always points toward the east (0°), and the angle increases counterclockwise from 0 to 2π. In this statistical analysis, we want to 1) show if the TCSD can be used to objectively locate the main regions of convection; and 2) understand when the TCSD indicates that the TC outflow is working against the environmental shear. We define strong environmental shear as the value that is larger than 10 m s^{-1}. Figure 10 uses the data that qualify for that definition. We also compare our results to the ''downshear left'' of total shear, which is often used to locate the main convection in a sheared TC. Only the raw data are shown here; smoothing was found to be unnecessary.

We first focus on North Atlantic hurricanes (maximum wind speed greater than 63 kt; upper panels in Fig. 10). Figure 10a shows the sample size distribution of the portion of convection between TCSD and environmental shear, as well as the portion of convection occupied by the downshear-left quadrant of the total shear vector. Here the portion of convection is defined as the ratio of the total number of convective grid points in the specified region divided by the total number of convective grid points in the whole region (defined as a disk of radius less than 3°). Note that Fig. 10 is essentially histograms that we group the data into bins. We use lines instead of bars here in order to compare different data clearly. It is clear from Fig. 10a that both methods are able to identify regions of high probability[4] with a sharp decrease of probability in both sides. For the downshear left of total shear method (red line in Fig. 10a), the value of the fraction of convection with the highest probability is about 30%, while for the region between the TCSD and environmental shear vectors, the fraction is about 55%, about twice as large as that of the downshear left of total shear. Thus, the region between the TCSD and the environmental shear usually identifies a substantially larger fraction of convection than the region downshear left of the total shear. We varied the definition of ''inner core'' regions, such as $r < 3°$, $0.5° < r < 3°$, and $r < 4°$ radially, and found that the result shown in Fig. 10a is not sensitive to these definitions (not shown).

Looking at the angle between TCSD and environmental shear in the blue line of Fig. 10b, it also exhibits a preferred value (with highest probability) of about 150°. This angle is consistent with our idealized simulations, in which the TCSD helps to resist the strong environmental shear. On the other hand, the total shear and environmental shear are usually parallel to each other (red line in Fig. 10b). Then is it possible that the larger preferred fraction of convection between TCSD and environmental shear than the downshear left of total shear (55% vs 30%) is just a result of larger angle (150° vs 90°)? Given that that 55%/150 is slightly larger than 30%/90, the azimuthal density of convection (percentage of convection per unit azimuthal angle) is slightly larger for regions between TCSD and environmental shear than downshear left of total shear. But using a more rigid standard to define convection (225 K instead of 250 K) does shift the highest probability of portion of convection from about 30% to close to 40% for the region of downshear left of total shear, while it does not change too much (55%) for the region between the TCSD and environmental shear (not shown). Since 55%/150 is smaller than 40%/90, the downshear left of total shear does seem to have denser strong convection than the region between TCSD and environmental shear, but the whole fraction of convection is still much larger in the latter (55%) than the former (40%). Therefore, we do think that the larger fraction of convection between TCSD and environmental shear is mainly due to the larger angle between them, compared with the downshear left of total shear, but it is necessary to get the region where convection is dense. Given the importance of the upshear-left convection on TC intensification (e.g., Rogers et al. 2016; Rios-Berrios et al. 2018), the above discussion indicates that the azimuthal region located upshear of the environmental shear should also be involved to study asymmetric convection. Also, although the total shear generally has a similar direction as the environmental shear (because the value of TCSD is generally small compared to the environmental shear, to be shown in Fig. 10c), the sharp distribution (high probability region) as shown in the blue line in Figs. 10a and 10b becomes much smoother if the environmental shear is replaced by the total shear (not shown). This suggests that the total shear is inherently a consequence of the environmental shear. The preferred magnitude of TCSD is about 5 m s^{-1} (blue line in Fig. 10c), whereas the total shear in nearly half of the sample is below 10 m s^{-1}, even though the environmental shear is always larger than 10 m s^{-1} (by our sample selection). Given these arguments, we conclude that the sample of North Atlantic hurricanes confirms the findings of our idealized simulations, namely, that the TCSD defines the lateral boundary of convection better than the downshear-left quadrant of total shear. Also, the TCSD prefers to be upshear left of the environmental shear, resisting strong environmental shear so that the total shear is reduced to a value that is no longer detrimental to intensification.

One question needs to be answered: are those samples that are near the highest probabilities in Figs. 10a–c connected with

[4] We use the sample size instead of the true probability here, in order for the different sample sizes to be seen clearly.

Unauthenticated | Downloaded 03/22/25 04:40 PM UTC

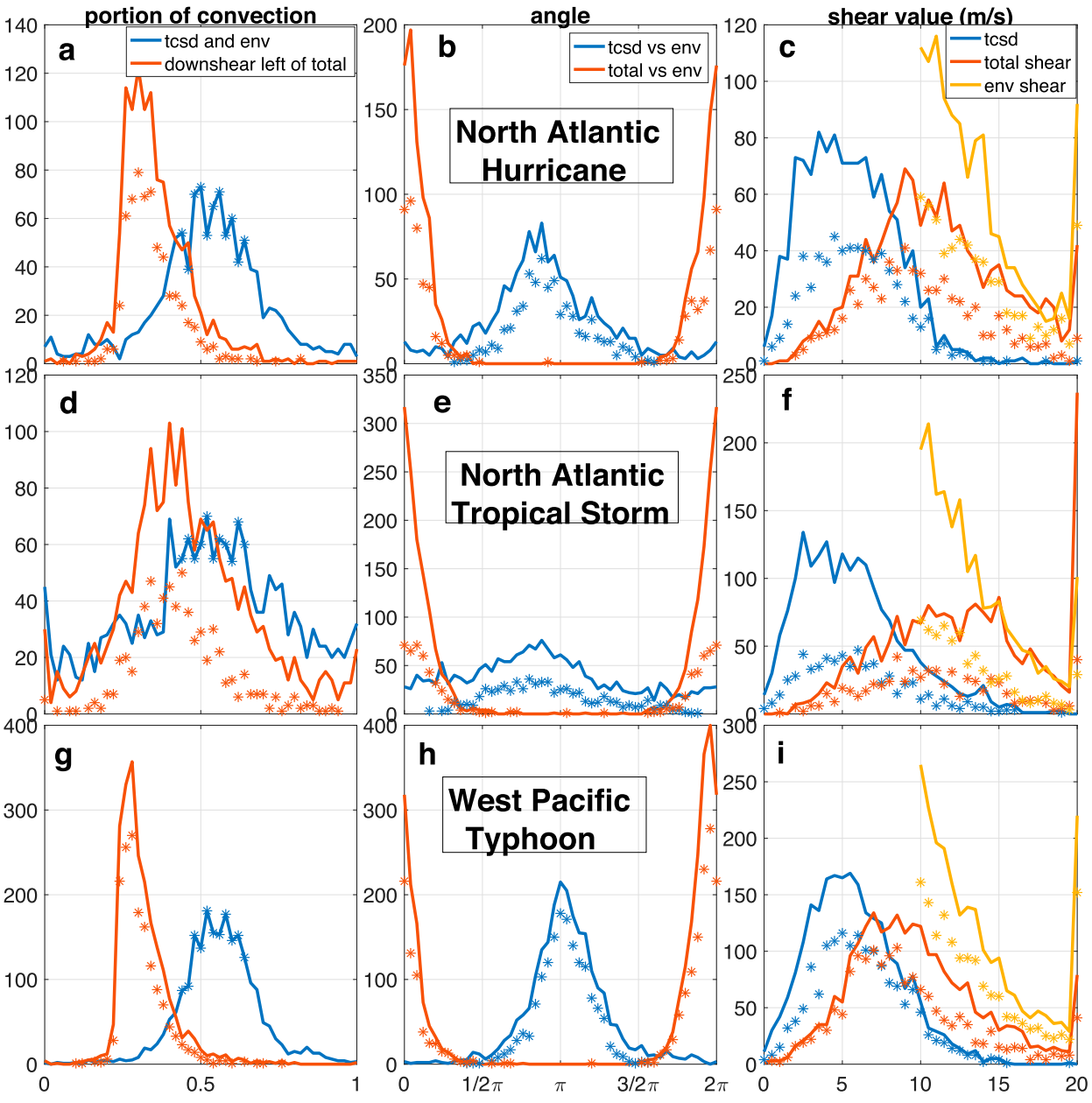

FIG. 10. Statistical analysis of TC data where the environmental shear magnitude is larger than 10 m s^{-1}. (a) Sample distribution of portion of convection for the region between TCSD and environmental shear (blue line), and for the region downshear left of total shear (red line). (b) Sample distribution of the angle between TCSD and environmental shear (blue line) and between total shear and environmental shear (red line). (c) Sample distribution of the magnitude of TCSD (blue line), total shear, (red line), and environmental shear (yellow line). Note that all the y axis represents sample size. The dotted data represent a subsample where the portion of convection surrounded by TCSD and environment shear vector is in the range [0.44, 0.66]. Data that are from (top) North Atlantic hurricane stage ($V_{max} > 63$ kt, sample size = 1178), (middle) North Atlantic tropical storm stage ($33 < V_{max} \leq 63$ kt, sample size = 1870), and (bottom) west Pacific typhoon stage (sample size = 2260).

each other? If so, one can confidently say that the data that are near the preferred azimuthal angle between TCSD and environmental shear (Fig. 10b) prefers to have TCSD with magnitude of about 5 m s^{-1} (Fig. 10c) and the portion of location of about 55% (Fig. 10a). We thus chose a subsample whose portion of convection in TCSD in Fig. 10a is within [0.44, 0.66]. Although its range is only about 20% of [0, 1], this subsample size includes more than half of the total sample (631 vs 1178). The corresponding result using this subsample is shown in stars with respective colors in Fig. 10. It is clear that the subsample with highest probabilities in the portion of convection (stars in Fig. 10a) is tightly connected to those with highest probabilities

Unauthenticated | Downloaded 03/22/25 04:40 PM UTC

for the angle (stars in Fig. 10b). Also, the angles between TCSD and environmental flow in the subsample are mostly within $[1/2\pi, 3/2\pi]$, indicating that the TCSD nearly always resists the environmental flow. Figure 10c shows that most of the samples with the smallest total shear ($<5\,m\,s^{-1}$) in the red line of Fig. 10c are those that have the highest probability of portion of convection (red stars in Fig. 10c where shear value is smaller than $5\,m\,s^{-1}$). Also, the subsample with highest probabilities of portion of convection (yellow stars in Fig. 10c) has a similar distribution of environmental shear compared with the whole sample (yellow line in Fig. 10c), implying that the preferred angle of TCSD (upshear left of environmental shear) is applicable to a wide range of the environmental shear values. Therefore, the high probability features in Figs. 10a–c are consistent with each other.

Finally, we test the dependence of the above findings on the strength of TCs and their locations. The middle panels of Fig. 10 are the results for North Atlantic TCs that only have tropical storm strength (maximum wind speed is between 34 and 63 kt). Generally, the middle panels and upper panels of Fig. 10 have similar patterns. The difference is that for tropical storms, the distribution is smoother, with less portion of data near the maximum probability (e.g., the blue lines in Fig. 10d vs Fig. 10a, and Fig. 10e vs Fig. 10b). Also, the portion of strong ($>10\,m\,s^{-1}$) total shear in Fig. 10f is more than that in Fig. 10c, although the distribution of environmental shear looks similar with each other (yellow lines in Figs. 10c,f). This suggests that the weaker the TC, the less able it is to resist strong environmental shear by TCSD. The lower panels of Fig. 10 show the results for western North Pacific typhoons (maximum wind speed larger than 63 kt). The findings for North Atlantic hurricanes are more clearly shown in samples of western North Pacific typhoons. Interestingly, the direction of TCSD and environmental shear are almost opposite to each other (the direction with the highest probability is π) in Fig. 10h, indicating a stronger resistance to environmental flow than North Atlantic hurricanes (the direction with the highest probability is about $5/6\pi$ in Fig. 10b, slightly less than π) if the magnitude of the TCSD is comparable. The portion of total shear that is smaller than $10\,m\,s^{-1}$ in Fig. 10i is the largest among the three different datasets. This is probably due to a larger sample size in the western North Pacific basin compared with the North Atlantic Ocean (note that the sample sizes for the upper, middle, and lower panels in Fig. 10 are 1178, 1870, and 2260, respectively), warmer SST in the western North Pacific, and different environmental flow structures in different regions. Last, we have also tested the moderately strong environmental shear ($5–10\,m\,s^{-1}$), and we found similar results (not shown) as in Fig. 10, suggesting that the results of TCSD are also applicable to moderately strong environmental shear.

b. Statistical relationship of TCSD with TC intensity change

This study mainly discusses TCSD as a resistance to strong environmental shear. We would like to know if TCSD can be used as a robust parameter to diagnose and predict the TC intensity change. Thus, we do a simple statistical analysis to test this idea.

We first correlate TCSD information with TC intensity change during the same time period. For simplicity, we only consider a time period of 72 h when computing correlations of TCSD-related parameters and TC intensity change. The ERA-Interim data of North Atlantic TCs between year 1980–2019 are used. All the TC strengths (tropical depression, tropical storm, and hurricane) are included in this analysis to get a large sample size. Not all the TCs that have TCSD will redevelop, because it depends on the angle between TCSD and environmental flow, as well as the strength of TCSD. Thus, a total of six parameters are used to correlate with TC intensity change. The first three are the magnitudes of total shear, environmental shear, and TCSD. The fourth parameter is the cosine of the angle between TCSD and environmental shear. The smaller value of cos (angle) indicates a larger resistance of TCSD to environmental shear, given the same magnitude of TCSD. The fifth parameter is the combination of the third and fourth parameters: $-$TCSD $\times$ cos(angle), which indicates the resistance of TCSD projected to the direction of environmental shear. The last parameter is the combination of the second and fifth parameters: environmental shear + TCSD $\times$ cos(angle). The last parameter gives the value of the "true" environmental shear after the TC impacts. All the six parameters use the 72 h time-averaged value. TC intensity change is indicated by the maximum wind speed difference between the last time and start time in the 72 h period. Last, we choose strong-environmental-shear cases where the 72-h mean environmental shear is larger than $10\,m\,s^{-1}$, giving us the total sample size of 2159.

The result is shown in Fig. 11, which displays the scatterplots of those parameters with intensity change, with correlation coefficients (R) and slope (K) of the best-fit line also shown. Among the parameters investigated, "env shear + TCSD $\times$ cos(angle)" is most strongly correlated with intensity change, with $R = -0.24$ (significance level larger than 99%). On the other hand, "env shear" is least correlated with intensity change, with $R = -0.07$. Interestingly, "total shear" ($R = -0.23$) is slightly less correlated with intensity change than "env shear + TCSD $\times$ cos(angle)." Also, the magnitude of the slope of "$-$tcsd $\times$ cos(angle)" ($K = 2.01$) is larger than that of total shear ($K = -1.65$), showing a robust signal of TCSD. Thus, incorporating TCSD information seems a promising tool for statistical forecasting of TC intensity change (more to be shown below). However, directly connecting the magnitude of TCSD with intensity change does not show much correlation (Fig. 11c, $R = -0.084$). TCSD needs to be combined with the "angle" (Fig. 11d, $R = -0.22$) to show the resistance (Fig. 11e, $R = 0.24$). Looking closely at the scatterplot of "cos (angle)" (Fig. 11d), although both the intensifying and decaying cases occur in the "upshear" of the environmental shear (range of cos (angle) is $[-1, 0]$), the number of intensifying cases is slightly larger. Likewise, the number of decaying cases for the "downshear" (range of cos (angle) is $[0, 1]$) is slightly larger than that of intensifying cases. Thus, while the direction of TCSD for the intensifying TCs is only slightly upshear of environmental shear, that value is statistically significant. Note that all the correlation coefficients in Fig. 11 passed the significance level of 99%.

Last, we correlate the same above parameters with future TC intensity change. As a first step, we average the shear

Unauthenticated | Downloaded 03/22/25 04:40 PM UTC

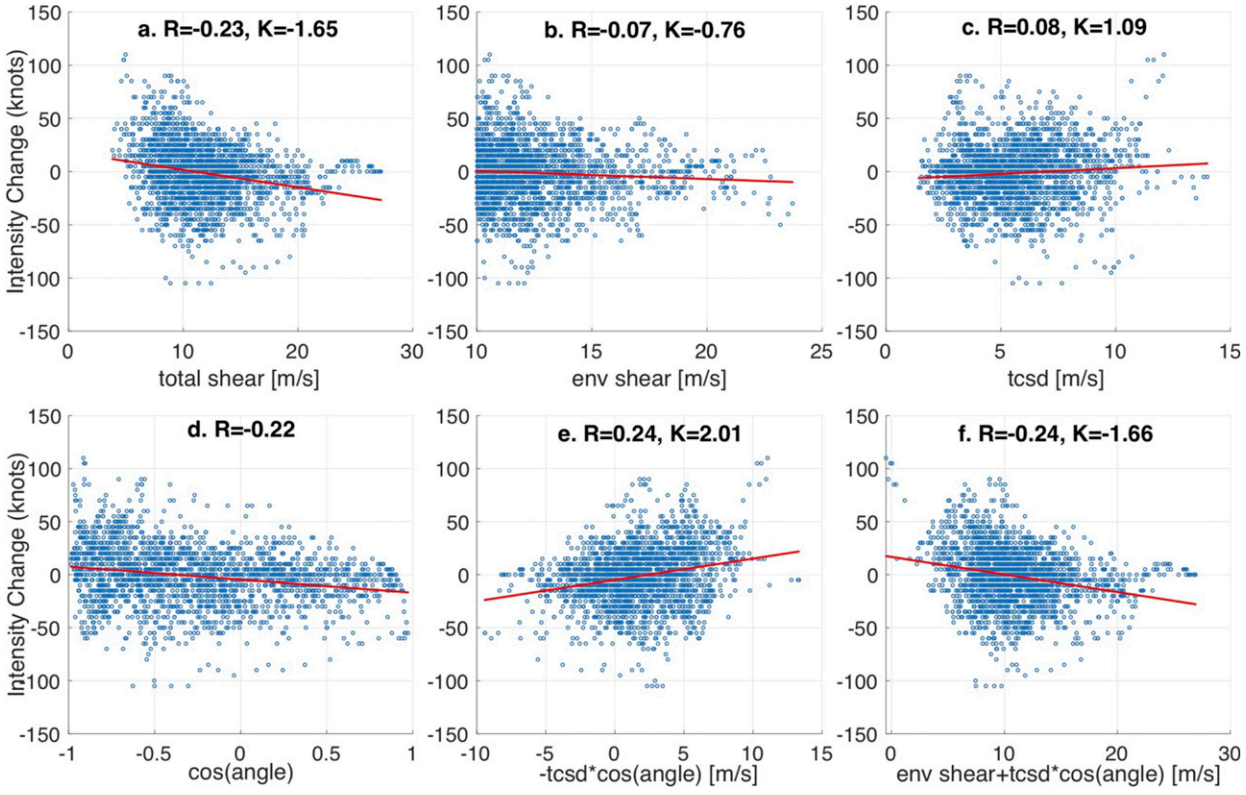

FIG. 11. Scatterplots of the 72-h TC intensity change (y axis) with (a) total shear, (b) environmental shear, (c) TCSD magnitude, (d) cosine of the angle between environmental shear and TCSD, (e) $-$TCSD $\times$ cos(angle), and (f) environmental shear + TCSD $\times$ cos(angle). The best-fit line is also shown in red in each subplot, with correlation coefficient (R) and slope of the best-fit line (K) shown at the top of each panel.

information over a short period of 12 h, and correlate them with the intensity change in the next 12 h. Same as above, we only choose data where environmental shear is larger than 10 m s^{-1}. We also divide the data based on TC intensity, with Vmax $\leq$ 63 kt (nonhurricanes) in Fig. 12, and Vmax $>$ 63 kt (hurricane) in Fig. 13. For nonhurricane TCs (Fig. 12), the best parameter to correlate future intensity change is "$-$TCSD $\times$ cos(angle)" with $R = 0.21$, better than total shear ($R = -0.15$). For hurricane TCs (Fig. 13), "$-$TCSD $\times$ cos(angle)" ($R = 0.23$) is not as well correlated with intensity change as total shear ($R = -0.30$), but "env shear + TCSD $\times$ cos(angle)" ($R = -0.31$) is slightly better correlated than total shear. The difference between weaker and stronger TCs might be due to the strong TCs already successfully resisting the shear. This can be inferred from Fig. 13d, where many more cases of TCSD are located upshear of the environmental shear [cos(angle) < 0] than downshear [cos(angle) > 0]. It is interesting to note that in Fig. 13d, for those with the largest intensity increase (at least 20 kt in 12 h), almost all of them are associated with an upshear-oriented TCSD. It is possible that such a shear configuration is especially important for RI, and this seems to agree with case studies of Edouard (2014) and Matthew (2016). Last, note that except for Fig. 12b (environmental shear in weak TCs), all the correlation coefficients in Figs. 12 and 13 passed the significance level of 99%.

In summary, our statistical analysis supports the idea that TCSD is an important indicator for TC intensity change and inner-core structure. However, the analysis here is just a first step to illustrate the importance of TCSD. More work is needed to test and confirm our results. For example, in addition to the IR temperature, we are interested in analyzing satellite data at other frequencies to define convection, such as the 85–91 GHz microwave temperature (e.g., Didlake et al. 2018). Also, reanalysis data with a higher temporal resolution are desired to get a larger sample.

5. Conclusions

In this study, we first investigated the resistance of a TC to strong environmental vertical wind shear using a recently developed idealized modeling framework. The time-varying point-downscaling method enables the smooth addition of environmental shear into a TC, and keeps the shear nearly constant with time after it is increased to a prescribed value. This new framework provides the ability to control the environmental shear and separate it from total shear, which is advantageous for studying the influence of environmental flow on TC structure and intensity change.

The TC-induced shear difference (TCSD), defined as the vector difference between the total shear and environmental

Unauthenticated | Downloaded 03/22/25 04:40 PM UTC

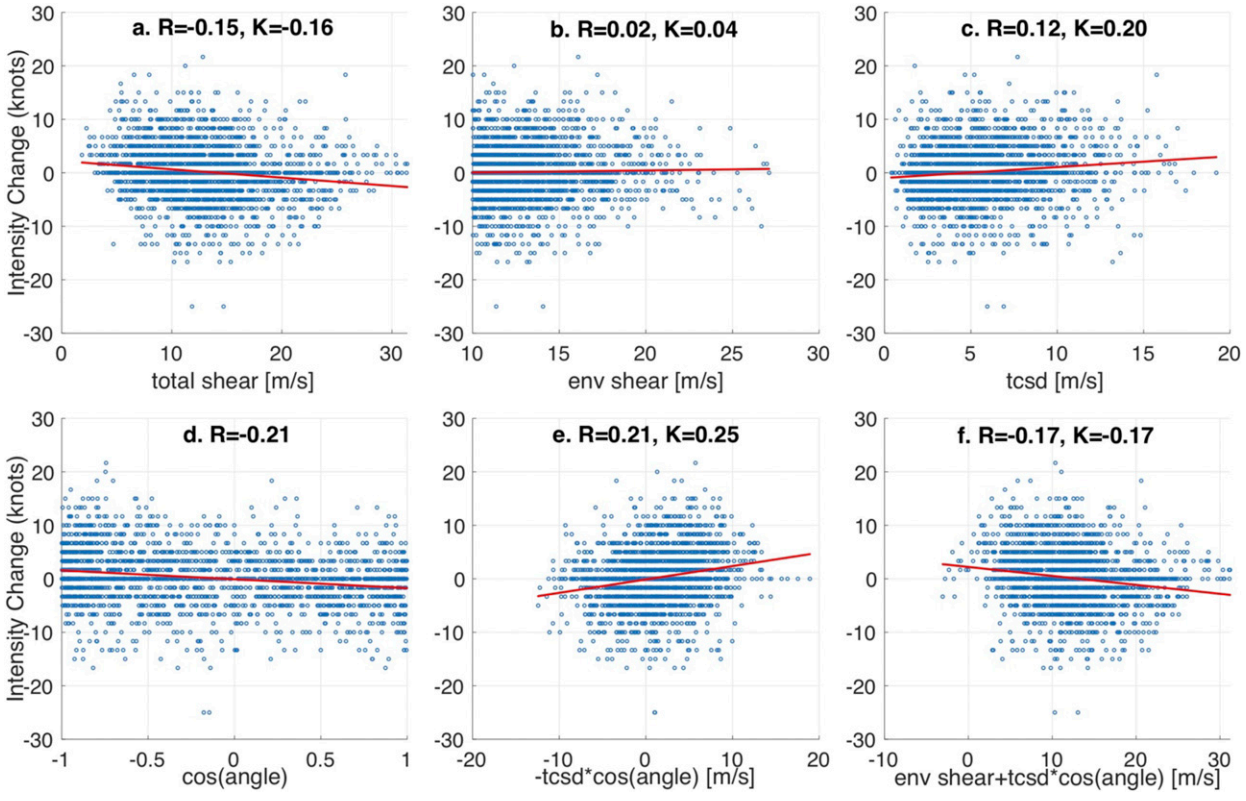

FIG. 12. As in Fig. 11, except for the correlation of 12-h mean shear information (x axis) with the next 12-h mean intensity change (y axis), for storms where Vmax $\leq$ 63 kt in the 24-h time period.

shear, is highlighted in this study. Via the TCSD, the total shear around the TC is weakened at the time of recovery. The TCSD is essentially a manifestation of the asymmetric TC flow, and particularly the upper-level outflow. The asymmetric outflow builds up when the westerly shear creates an inertially less stable region in the upshear-left quadrant relative to the environmental shear. When the outflow is able to significantly resist the environmental flow, the TC starts to recover.

A mesoscale forced downdraft is located just below where the upper-level enhanced outflow and environmental flow converge (see convergence in Fig. 4c). We thus hypothesize that the forced downdraft is due to the dynamic forcing by upper-level flow convergence as well as the diabatic cooling. The forced downdraft is very strong (maximum strength is stronger than $-10\,\mathrm{m\,s^{-1}}$) and descends to the lower boundary layer, thereby greatly affecting the inner-core structure and intensity. The forced downdraft is adjacent to the rainband convection, making it a lateral boundary of the rainband. Because the enhanced outflow, the forced downdraft, and the rainband are all coupled features, the TCSD also represents the location of the forced downdraft.

We found that the TCSD can help explain TC intensification under strong environmental shear. Hurricanes Edouard (2014) and Matthew (2016) are two examples that support this argument: they experienced rapid intensification under strong environmental shear, and in both cases the TCSD vector was pointing against the environmental shear. Moreover, the direction of the TCSD (because of the downdraft) defines the azimuthal range of the asymmetric convection. Therefore, TCSD together with the environmental shear might be better correlated with the azimuthal range of the asymmetric convection.

A statistical analysis that covers the Northern Hemisphere hurricane seasons between 1980 and 2019 confirms the findings from our idealized simulations, that the majority of convection is located between TCSD and the environmental shear vector, with the angle mainly within $[1/2\pi, 3/2\pi]$. Such a TCSD configuration might help TCs resist strong environmental shear so that the total shear is decreased and TCs can sometimes develop under strong environmental shear. The above findings are neither qualitatively sensitive to different TC strength (hurricane vs tropical storm), nor to different TC locations (North Atlantic vs west Pacific). However, it is noteworthy that weaker TCs generally have a weaker signal (local maxima of probability in Fig. 10) of TCSD. Also, the sample of western North Pacific typhoons has a stronger signal of TCSD than that of the North Atlantic hurricanes.

A real TC might not experience such strong weakening and recovery as seen in our idealized simulation, because the environmental flow can be modulated by a TC in the real world. The recovery of a real TC under strong shear could also be affected by low SST and large midtroposphere saturation deficit that can create stronger downdrafts. By introducing

Unauthenticated | Downloaded 03/22/25 04:40 PM UTC

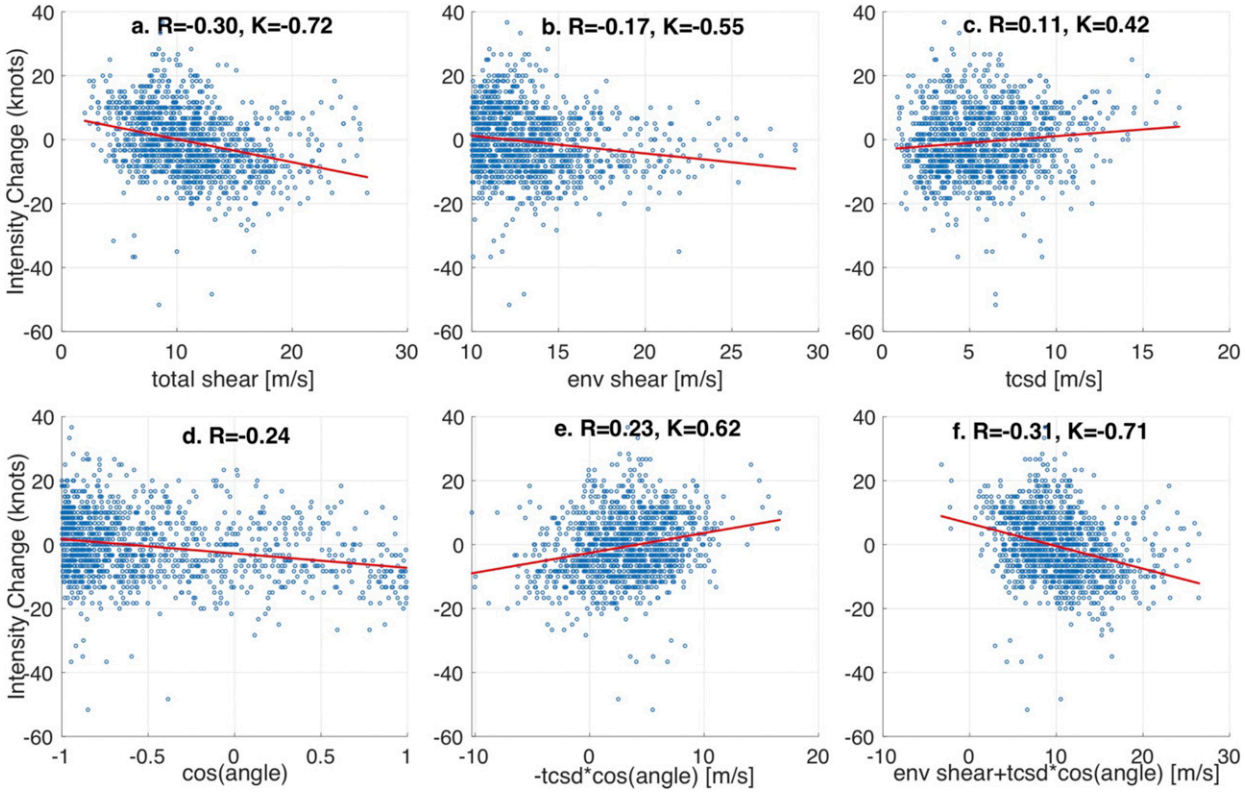

FIG. 13. As in Fig. 12, but for storms where Vmax > 63 kt.

TCSD, we hope to have presented a better understanding of the interaction between strong environmental shear and the TC, and the consequent effects on TC intensity and structure. The TC asymmetric features (such as the upper-level asymmetric outflow) that are induced by environmental shear might in turn help resist strong environmental shear. More work is needed to study the applicability of TCSD to TC intensity and structure forecasts. For example, in these and many similar model simulations, the vertical resolution near the outflow layer is not very good. Increasing the number of vertical levels in the outflow region may lead to more physically realistic results. Observationally, we would like to use different data (such as the microwave imagery) to test the relationship between TCSD and TC intensity and structure. Also, dropsondes from high-altitude aircraft released in the upshear-left quadrant could possibly provide insight on the structure of the shear and dry air upshear.

Acknowledgments. This study was supported by the Office of Naval Research Grant N000141410115. The authors also acknowledge helpful discussions with Brian Mapes, Robert Rogers, and Mohamed Iskandarani and computational support from the University of Miami Center for Computational Science. The first author also acknowledges Matthew Onderlinde for the help of TVPDS technique and Peter Finocchio for providing DDS and SUS shear profiles. The authors also thank Dr. Will Komaromi and two anonymous reviewers for the helpful comments.

Data availability statement. All the model and reanalysis data for this study are stored in the hard drives belonging to the University of Miami, and are available upon request.

REFERENCES

Alvey, G. R., E. Zipser, and J. Zawislak, 2020: How does Hurricane Edouard (2014) evolve toward symmetry before rapid intensification? A high-resolution ensemble study. *J. Atmos. Sci.*, **77**, 1329–1351, https://doi.org/10.1175/JAS-D-18-0355.1.

Black, M. L., R. W. Burpee, and F. D. Marks Jr., 1996: Vertical motion characteristics of tropical cyclones determined with airborne Doppler radial velocities. *J. Atmos. Sci.*, **53**, 1887–1909, https://doi.org/10.1175/1520-0469(1996)053<1887:VMCOTC>2.0.CO;2.

——, J. F. Gamache, F. D. Marks, C. Samsury, and H. E. Willoughby, 2002: Eastern Pacific Hurricanes Jimena of 1991 and Olivia of 1994: The effect of vertical shear on structure and intensity. *Mon. Wea. Rev.*, **130**, 2291–2312, https://doi.org/10.1175/1520-0493(2002)130<2291:EPHJOA>2.0.CO;2.

Corbosiero, K. L., and J. Molinari, 2002: The effects of vertical wind shear on the distribution of convection in tropical cyclones. *Mon. Wea. Rev.*, **130**, 2110–2123, https://doi.org/10.1175/1520-0493(2002)130<2110:TEOVWS>2.0.CO;2.

Dai, Y., S. J. Majumdar, and D. S. Nolan, 2017: Secondary eyewall formation in tropical cyclones by outflow–jet interaction. *J. Atmos. Sci.*, **74**, 1941–1958, https://doi.org/10.1175/JAS-D-16-0322.1.

——, ——, and ——, 2019: The outflow–rainband relationship induced by environmental flow around tropical cyclones.

Unauthenticated | Downloaded 03/22/25 04:40 PM UTC

J. Atmos. Sci., **76**, 1845–1863, https://doi.org/10.1175/JAS-D-18-0208.1.

Davis, C. A., S. C. Jones, and M. Riemer, 2008: Hurricane vortex dynamics during Atlantic extratropical transition. *J. Atmos. Sci.*, **65**, 714–736, https://doi.org/10.1175/2007JAS2488.1.

Dee, D. P., and Coauthors, 2011: The ERA-Interim reanalysis: Configuration and performance of the data assimilation system. *Quart. J. Roy. Meteor. Soc.*, **137**, 553–597, https://doi.org/10.1002/qj.828.

DeMaria, M., 1996: The effect of vertical shear on tropical cyclone intensity change. *J. Atmos. Sci.*, **53**, 2076–2088, https://doi.org/10.1175/1520-0469(1996)053<2076:TEOVSO>2.0.CO;2.

Didlake, A. C., P. D. Reasor, R. F. Rogers, and W. Lee, 2018: Dynamics of the transition from spiral rainbands to a secondary eyewall in Hurricane Earl (2010). *J. Atmos. Sci.*, **75**, 2909–2929, https://doi.org/10.1175/JAS-D-17-0348.1.

Dunion, J. P., 2011: Rewriting the climatology of the tropical North Atlantic and Caribbean Sea atmosphere. *J. Climate*, **24**, 893–908, https://doi.org/10.1175/2010JCLI3496.1.

Elsberry, R. L., and R. A. Jefferies, 1996: Vertical wind shear influences on tropical cyclone formation and intensification during TCM-92 and TCM-93. *Mon. Wea. Rev.*, **124**, 1374–1387, https://doi.org/10.1175/1520-0493(1996)124<1374:VWSIOT>2.0.CO;2.

Finocchio, P. M., and S. J. Majumdar, 2017a: The predictability of idealized tropical cyclones in environments with time-varying vertical wind shear. *J. Adv. Model. Earth Syst.*, **9**, 2836–2862, https://doi.org/10.1002/2017MS001168.

——, and ——, 2017b: A statistical perspective on wind profiles and vertical wind shear in tropical cyclone environments. *Mon. Wea. Rev.*, **145**, 361–378, https://doi.org/10.1175/MWR-D-16-0221.1.

——, ——, D. S. Nolan, and M. Iskandarani, 2016: Idealized tropical cyclone responses to the height and depth of environmental vertical wind shear. *Mon. Wea. Rev.*, **144**, 2155–2175, https://doi.org/10.1175/MWR-D-15-0320.1.

Fischer, M. S., B. H. Tang, and K. L. Corbosiero, 2017: Assessing the influence of upper-tropospheric troughs on tropical cyclone intensification rates after genesis. *Mon. Wea. Rev.*, **145**, 1295–1313, https://doi.org/10.1175/MWR-D-16-0275.1.

Frank, W. M., and E. A. Ritchie, 2001: Effects of vertical wind shear on the intensity and structure of numerically simulated hurricanes. *Mon. Wea. Rev.*, **129**, 2249–2269, https://doi.org/10.1175/1520-0493(2001)129<2249:EOVWSO>2.0.CO;2.

Guimond, S. R., G. M. Heymsfield, and F. J. Turk, 2010: Multiscale observations of Hurricane Dennis (2005): The effects of hot towers on rapid intensification. *J. Atmos. Sci.*, **67**, 633–654, https://doi.org/10.1175/2009JAS3119.1.

Hong, S.-Y., and J.-O. J. Lim, 2006: The WRF single-moment 6-class microphysics scheme (WSM6). *J. Korean Meteor. Soc.*, **42**, 129–151.

——, Y. Noh, and J. Dudhia, 2006: A new vertical diffusion package with an explicit treatment of entrainment processes. *Mon. Wea. Rev.*, **134**, 2318–2341, https://doi.org/10.1175/MWR3199.1.

Jones, S. C., 1995: The evolution of vortices in vertical shear: I: Initially barotropic vortices. *Quart. J. Roy. Meteor. Soc.*, **121**, 821–851, https://doi.org/10.1002/qj.49712152406.

Knapp, K. R., and Coauthors, 2014: NOAA Climate Data Record (CDR) of Gridded Satellite Data from ISCCP B1 (GridSat-B1) Infrared Channel Brightness Temperature, version 2. NOAA National Centers for Environmental Information, https://doi.org/10.7289/V59P2ZKR.

Komaromi, W. A., and J. D. Doyle, 2017: Tropical cyclone outflow and warm core structure as revealed by HS3 dropsonde data. *Mon. Wea. Rev.*, **145**, 1339–1359, https://doi.org/10.1175/MWR-D-16-0172.1.

——, and ——, 2018: On the dynamics of tropical cyclone and trough interactions. *J. Atmos. Sci.*, **75**, 2687–2709, https://doi.org/10.1175/JAS-D-17-0272.1.

Miyamoto, Y., and D. S. Nolan, 2018: Structural changes preceding rapid intensification in tropical cyclones as shown in a large ensemble of idealized simulations. *J. Atmos. Sci.*, **75**, 555–569, https://doi.org/10.1175/JAS-D-17-0177.1.

Molinari, J., and D. Vollaro, 2010: Rapid intensification of a sheared tropical storm. *Mon. Wea. Rev.*, **138**, 3869–3885, https://doi.org/10.1175/2010MWR3378.1.

Nguyen, L. T., R. F. Rogers, and P. D. Reasor, 2017: Thermodynamic and kinematic influences on precipitation symmetry in sheared tropical cyclones: Bertha and Cristobal (2014). *Mon. Wea. Rev.*, **145**, 4423–4446, https://doi.org/10.1175/MWR-D-17-0073.1.

Nolan, D. S., 2011: Evaluating environmental favorableness for tropical cyclone development with the method of point downscaling. *J. Adv. Model. Earth Syst.*, **3**, M08001, https://doi.org/10.1029/2011MS000063.

——, Y. Moon, and D. P. Stern, 2007: Tropical cyclone intensification from asymmetric convection: Energetics and efficiency. *J. Atmos. Sci.*, **64**, 3377–3405, https://doi.org/10.1175/JAS3988.1.

Onderlinde, M. J., and D. S. Nolan, 2017: The tropical cyclone response to changing wind shear using the method of time-varying point-downscaling. *J. Adv. Model. Earth Syst.*, **9**, 908–931, https://doi.org/10.1002/2016MS000796.

Paterson, L. A., B. N. Hanstrum, N. E. Davidson, and H. C. Weber, 2005: Influence of environmental vertical wind shear on the intensity of hurricane-strength tropical cyclones in the Australian region. *Mon. Wea. Rev.*, **133**, 3644–3660, https://doi.org/10.1175/MWR3041.1.

Reasor, P. D., and M. D. Eastin, 2012: Rapidly intensifying Hurricane Guillermo (1997). Part II: Resilience in shear. *Mon. Wea. Rev.*, **140**, 425–444, https://doi.org/10.1175/MWR-D-11-00080.1.

——, M. T. Montgomery, F. D. Marks Jr., and J. F. Gamache, 2000: Low-wavenumber structure and evolution of the hurricane inner core observed by airborne dual-Doppler radar. *Mon. Wea. Rev.*, **128**, 1653–1680, https://doi.org/10.1175/1520-0493(2000)128<1653:LWSAEO>2.0.CO;2.

——, ——, and L. D. Grasso, 2004: A new look at the problem of tropical cyclones in vertical shear flow: Vortex resiliency. *J. Atmos. Sci.*, **61**, 3–22, https://doi.org/10.1175/1520-0469(2004)061<0003:ANLATP>2.0.CO;2.

——, R. Rogers, and S. Lorsolo, 2013: Environmental flow impacts on tropical cyclone structure diagnosed from airborne Doppler radar composites. *Mon. Wea. Rev.*, **141**, 2949–2969, https://doi.org/10.1175/MWR-D-12-00334.1.

Riemer, M., M. T. Montgomery, and M. E. Nicholls, 2010: A new paradigm for intensity modification of tropical cyclones: Thermodynamic impact of vertical wind shear on the inflow layer. *Atmos. Chem. Phys.*, **10**, 3163–3188, https://doi.org/10.5194/acp-10-3163-2010.

Rios-Berrios, R., and R. D. Torn, 2017: Climatological analysis of tropical cyclone intensity changes under moderate vertical wind shear. *Mon. Wea. Rev.*, **145**, 1717–1738, https://doi.org/10.1175/MWR-D-16-0350.1.

——, ——, and C. A. Davis, 2016: An ensemble approach to investigate tropical cyclone intensification in sheared environments. Part I: Katia (2011). *J. Atmos. Sci.*, **73**, 71–93, https://doi.org/10.1175/JAS-D-15-0052.1.

Unauthenticated | Downloaded 03/22/25 04:40 PM UTC

——, C. A. Davis, and R. D. Torn, 2018: A hypothesis for the intensification of tropical cyclones under moderate vertical wind shear. *J. Atmos. Sci.*, **75**, 4149–4173, https://doi.org/10.1175/JAS-D-18-0070.1.

Rogers, R., S. S. Chen, J. Tenerelli, and H. Willoughby, 2003: A numerical study of the impact of vertical shear on the distribution of rainfall in Hurricane Bonnie (1998). *Mon. Wea. Rev.*, **131**, 1577–1599, https://doi.org/10.1175//2546.1.

——, S. Lorsolo, P. Reasor, J. Gamache, and F. Marks, 2012: Multiscale analysis of tropical cyclone kinematic structure from airborne Doppler radar composites. *Mon. Wea. Rev.*, **140**, 77–99, https://doi.org/10.1175/MWR-D-10-05075.1.

——, J. A. Zhang, J. Zawislak, H. Jiang, G. R. Alvey III, E. J. Zipser, and S. N. Stevenson, 2016: Observations of the structure and evolution of Hurricane Edouard (2014) during intensity change. Part II: Kinematic structure and the distribution of deep convection. *Mon. Wea. Rev.*, **144**, 3355–3376, https://doi.org/10.1175/MWR-D-16-0017.1.

Ryglicki, D. R., J. H. Cossuth, D. Hodyss, and J. D. Doyle, 2018: The unexpected rapid intensification of tropical cyclones in moderate vertical wind shear. Part I: Overview and observations. *Mon. Wea. Rev.*, **146**, 3773–3800, https://doi.org/10.1175/MWR-D-18-0020.1.

——, J. D. Doyle, D. Hodyss, J. H. Cossuth, Y. Jin, K. C. Viner, and J. M. Schmidt, 2019: The unexpected rapid intensification of tropical cyclones in moderate vertical wind shear. Part III: Outflow–environment interaction. *Mon. Wea. Rev.*, **147**, 2919–2940, https://doi.org/10.1175/MWR-D-18-0370.1.

Simpson, R. H., and H. Riehl, 1958: Mid-tropospheric ventilation as a constraint on hurricane development and maintenance. *Proc. Tech. Conf. on Hurricanes*, Amer. Meteor. Soc., Miami, FL, D4.1–D4.10.

Skamarock, W. C., and Coauthors, 2008: A description of the Advanced Research WRF version 3. NCAR Tech. Note NCAR/TN-4751STR, 113 pp.

Stauffer, D. R., and N. L. Seaman, 1990: Use of four-dimensional data assimilation in a limited-area mesoscale model. Part I: Experiments with synoptic-scale data. *Mon. Wea. Rev.*, **118**, 1250–1277, https://doi.org/10.1175/1520-0493(1990)118<1250:UOFDDA>2.0.CO;2.

Stewart, S. R., 2014: National Hurricane Center Tropical Cyclone Report: Hurricane Edouard (28 September–9 October 2016). National Hurricane Center Rep. AL142016, 19 pp., https://www.nhc.noaa.gov/data/tcr/AL062014_Edouard.pdf.

——, 2017: National Hurricane Center Tropical Cyclone Report: Hurricane Matthew (11-19 September 2016). National Hurricane Center Rep. AL062014, 96 pp., https://www.nhc.noaa.gov/data/tcr/AL142016_Matthew.pdf.

Tang, B., and K. A. Emanuel, 2010: Midlevel ventilation's constraint on tropical cyclone intensity. *J. Atmos. Sci.*, **67**, 1817–1830, https://doi.org/10.1175/2010JAS3318.1.

Velden, C. S., C. M. Hayden, S. J. Nieman, W. P. Menzel, S. Wanzong, and J. S. Goerss, 1997: Upper-tropospheric winds derived from geostationary satellite water vapor observations. *Bull. Amer. Meteor. Soc.*, **78**, 173–196, https://doi.org/10.1175/1520-0477(1997)078<0173:UTWDFG>2.0.CO;2.

Zawislak, J., H. Jiang, G. R. Alvey, E. J. Zipser, R. F. Rogers, J. A. Zhang, and S. N. Stevenson, 2016: Observations of the structure and evolution of Hurricane Edouard (2014) during intensity change. Part I: Relationship between the thermodynamic structure and precipitation. *Mon. Wea. Rev.*, **144**, 3333–3354, https://doi.org/10.1175/MWR-D-16-0018.1.

Zhang, D.-L., and C. Q. Kieu, 2005: Shear-forced vertical circulations in tropical cyclones. *Geophys. Res. Lett.*, **32**, L13822, https://doi.org/10.1029/2005GL023146.

Zhang, F., and D. Tao, 2013: Effects of vertical wind shear on the predictability of tropical cyclones. *J. Atmos. Sci.*, **70**, 975–983, https://doi.org/10.1175/JAS-D-12-0133.1.

Unauthenticated | Downloaded 03/22/25 04:40 PM UTC